

**KERNFORSCHUNGSZENTRUM**

**KARLSRUHE**

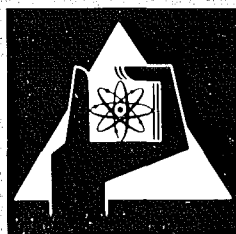
Oktober 1974

KFK 2063

Institut für Angewandte Kernphysik  
Projekt Schneller Brüter

keV Neutron Radiative Capture and Total Cross Section  
of  $^{50,52,53}\text{Cr}$ ,  $^{54,57}\text{Fe}$ , and  $^{62,64}\text{Ni}$

H. Beer, R.R. Spencer



**GESELLSCHAFT  
FÜR  
KERNFORSCHUNG M.B.H.**

**KARLSRUHE**

Als Manuskript vervielfältigt

Für diesen Bericht behalten wir uns alle Rechte vor

GESELLSCHAFT FÜR KERNFORSCHUNG M. B. H.  
KARLSRUHE

KERNFORSCHUNGSZENTRUM KARLSRUHE

KFK 2063

Institut für Angewandte Kernphysik  
Projekt Schneller Brüter

KeV NEUTRON RADIATIVE CAPTURE AND  
TOTAL CROSS SECTION OF  $^{50,52,53}\text{Cr}$ ,  
 $^{54,57}\text{Fe}$ , AND  $^{62,64}\text{Ni}$

H. Beer and R.R. Spencer<sup>+</sup>

<sup>+</sup>On leave from Kernforschungszentrum Karlsruhe, Germany

Gesellschaft für Kernforschung mbH, Karlsruhe



## ABSTRACT

Enriched samples of  $^{50,52,53}\text{Cr}$ ,  $^{54,57}\text{Fe}$  and  $^{62,64}\text{Ni}$  were measured in capture and with the exception of  $^{53}\text{Cr}$  and  $^{57}\text{Fe}$  in transmission in the energy ranges 5-200 keV and 10-300 keV, respectively. The capture and total cross section data analyzed provided resonance parameters for both s- and  $\ell > 0$  wave resonances. s- and p-wave strength functions were determined and neutron width and level spacing distributions established. A positive correlation was found between the radiation widths and the reduced neutron widths.

keV-Neutroneneinfang- und totaler Querschnitt von  $^{50,52,53}\text{Cr}$ ,  $^{54,57}\text{Fe}$  und  $^{62,64}\text{Ni}$

## ZUSAMMENFASSUNG

Mit angereicherten Proben von  $^{50,52,53}\text{Cr}$ ,  $^{54,57}\text{Fe}$  und  $^{62,64}\text{Ni}$  wurden der Einfangquerschnitt und mit Ausnahme von  $^{53}\text{Cr}$  und  $^{57}\text{Fe}$  der totale Querschnitt in den Energiebereichen 5-200 keV bzw. 10-300 keV gemessen. Die analysierten Einfang- und totalen Querschnittsdaten lieferten Resonanzparameter für s und  $\ell > 0$  Wellen Resonanzen. s- und p-Wellen Stärkefunktionen wurden bestimmt und Verteilungen für Niveaubreiten und Niveauabstände aufgestellt. Eine positive Korrelation zwischen den Strahlungsbreiten und den reduzierten Neutronenbreiten wurde gefunden.

## 1. INTRODUCTION

The Karlsruhe 3 MV pulsed Van de Graaff has been used in a program of capture and transmission measurements to study the keV neutron cross sections of medium weight nuclei. Particular emphasis has been placed on the isotopes of iron, chromium and nickel, which are the major constituents of stainless steel and therefore of importance in the calculation of neutron economy for the fast breeder project. The resonance structure of the cross sections analyzed provided resonance parameters which were applied to establish width and spacing distributions and to search for possible correlations between radiation widths and reduced neutron widths. For both s- and p-wave resonances strength functions were determined, which are of interest for optical model calculations. Together with the work of previous investigations at Karlsruhe (1) - (9), the present capture and transmission measurements give resonance parameters for all the stable isotopes of chromium, iron and nickel except  $^{58}\text{Fe}$  and  $^{54}\text{Cr}$  which are relatively low in abundance.

The transmission data are analyzed using a multi-level, R-matrix formalism to derive the energies and neutron widths of s-wave resonances. Due to the occurrence of strong interference effects in the data the multi-level approach has been a necessity in obtaining proper fits to the data. These neutron widths are then used along with an area analysis of the corresponding resonances observed in the capture experiments to derive the total radiation widths. Because of the much greater resonance density observed in capture measurements (i.e. the capture method is much more sensitive to higher l-wave effects) careful attention must be accorded to the establishment of energy scales in the two types of experiments. Hence, it has been found preferable to carry out both measurements under similar experimental conditions. The use of enriched isotopic samples is also a necessity particularly in the capture measurements where resonance densities are higher and the energy resolution not as high.

## 2. EXPERIMENT

The transmission and capture measurements were carried out by the time-of-flight technique. Neutrons were produced at the Karlsruhe 3 MV Van-de-Graaff-accelerator, by means of the  ${}^7\text{Li}(p,n){}^7\text{Be}$  reaction in a thick ( $\approx 100$  keV) lithium target with 1 ns wide proton bursts and repetition frequencies of 250 and 500 kHz for transmission and capture, respectively.

In both measurements the neutron beam was carefully collimated to fall within the sample area. In the capture measurement, the sample to be analyzed was interchanged with a carbon sample and a gold sample for background and neutron flux determination, respectively. In the transmission measurement, two samples different in thickness and an empty sample container were successively brought into the neutron beam. The sample cycling to average out fluctuations in neutron intensity was controlled by a proton beam current integrator.

In the transmission experiment a 4 3/8" dia. x 1/2" thick  ${}^6\text{Li}$  loaded glass scintillator detector (10) was installed at a neutron flight path of 4.96 m to detect the transmitted neutrons. Flight time spectra of the neutrons were recorded via a Laben digital time sorter and stored in a CAE 510 on-line computer into 2048 channel arrays. The overall time resolution was 0.6 ns/m.

In the capture measurement, the neutron capture events of the sample were detected via the prompt capture  $\gamma$ -rays with a scintillator tank at a neutron flight path of 2 m. The Karlsruhe tank is 1.1 m diameter, contains 800 liters of liquid scintillator and has a 10 cm diameter through-hole for placement of the sample at the tank center. A more detailed description can be found elsewhere (11). The data consisted of all  $\gamma$ -ray events between about 3 MeV and an energy well above the neutron binding energy of the sample. They were stored on-line in a CAE 510 computer for each sample position into an 8 x 512 channel, pulse height versus time array. The lower threshold of 3 MeV is set in order to avoid any effects due to the 2.2 MeV  $\gamma$ -ray resulting from capture of scattered neutrons in the hydrogen of the scintillator. The overall time resolution of the system was 2 ns/m.

The samples to be analyzed consisted of powdered oxides or powdered metal of enriched isotopes. The sample thicknesses and the isotopic composition of all samples are given in Table 1. For the transmission measurement, the sample material was placed in thin-walled aluminum containers of 1.1 cm diameter. For the capture measurement, the sample material was pressed into flat cylindrical bronze containers with a diameter of 8 cm. Because of the small amount of  $^{64}\text{Ni}$  available a bronze container of 4.5 cm diameter had to be used. The gold sample was a disc of 9 cm dia. x .1 cm thickness. The carbon samples were graphite discs chosen to match the scattering cross section of the analyzed sample.

### 3. DATA REDUCTIONS AND RESULTS

#### 3.1 Transmission Measurement

Transmissions and their statistical uncertainties were computed from data by means of the FORTRAN IV code TRAMI (12). The sample and open backgrounds for these calculations are determined from the counts in the sample and open spectra, respectively, in a region between the  $\gamma$  peak and the onset of the fastest neutrons. Chi-square fits to the transmission data were then calculated using an R-matrix formalism such as described by Lane and Thomas (13). These fits and the final plotting routines were carried out by means of the code FANAL II (14). The program takes into account a correction for the contaminants and the resolution broadening and delivers the resonance parameters. For the resolution broadening, a Gaussian function was used. Doppler broadening was assumed to be negligible for most of the broad s-wave resonances. Neutron energies were computed from their time-of-flight, using the  $\gamma$ -ray peak position to determine time zero. In the case of the oxide samples, the oxygen cross section was included by means of a potential scattering radius of 5.6 fermis as a contaminant input. This produced a slightly energy dependent cross section for oxygen below 300 keV which is in good agreement with the data of Mooring et al. (15).

The resulting best fits to the transmission data are shown with the measured thick and thin sample data points in Figures 1-16. For the sake of clarity error bars indicating the statistical uncertainty in the measured data were plotted for every 10<sup>th</sup> or 20<sup>th</sup> point, only. Plots of the resolution-

broadened total cross section for the pure isotopes are included in the figures, too. The values and estimated errors for the resonance energies,  $E_0$ , and the neutron widths,  $\Gamma_n$  (or  $g \Gamma_n$  for  $l > 0$ ) are listed in the Tables 2-15. Also given are values of  $a_J$ , the s-wave potential scattering radius, and  $S_J'$ , a parameter which describes the effect of distant resonances.  $S_J'$  is the strength function of a "Picket Fence" model which assumes equally spaced resonances of equal widths outside the region of analysis. For the sake of completeness with regard to the measured capture cross section of  $^{53}\text{Cr}$  and  $^{57}\text{Fe}$  the respective transmission data of Rohr et al. (3) and Müller et al. (6) were included, too.

### 3.2 Capture Measurement

Values of capture yields per sample thickness are computed from the counts per channel data, after summing the appropriate pulse height channels, by means of the following formula:

$$" \sigma_{\gamma} " = \frac{C_S - C_{SX}}{C_A - C_{SA}} \times \frac{N_A}{N_X} \times \frac{\epsilon_A}{\epsilon_X} \times \sigma_{\gamma A} \quad (1)$$

where  $C_X$ ,  $C_A$  are counts per channel for the sample and the gold standard, respectively.  $N_X$ ,  $N_A$  are the sample thicknesses,  $\epsilon_X$ ,  $\epsilon_A$  are the spectrum fractions for sample and gold.  $C_{SA}$ ,  $C_{SX}$  are backgrounds and  $\sigma_{\gamma A}$  is the gold capture standard cross section (11). Energies corresponding to each time-of-flight channel are computed from the measured flight path and the time of each channel relative to the position of the "prompt"  $\gamma$ -ray peak from the lithium target.

The spectrum fractions used are in general an average for each sample and result from the lack of data below our 3 MeV pulse height threshold. Since the shape of this spectrum below threshold is unknown an assumption as to its shape must be made and a liberal error, usually of the order of 10 %, is assigned to these values.

The overall error of the capture yield, which includes the statistical error in the gold cross section and the error in the spectrum fraction, is computed for each channel. Plots of the capture yields of the nuclei are shown in the Fig. 1-16 together with the corresponding total cross section of the trans-

mission experiments (the total and capture cross section values can be requested from the neutron data center at Saclay, CCDN, B.P. 9, F-91 Gif-sur-Yvette, France).

The complexity of the capture data are somewhat startling in comparison to the total cross section plots and suggest that the capture cross sections of some of the less abundant isotopes should be considered in computations of the capture for the natural material. It is also apparent that p-waves and perhaps higher l-wave capture is an important effect.

The last phase of data reduction consists of area analysis of the resolved resonances. Integrated capture yields per nucleon are determined for each resonance. For ideal thin targets these areas are equal to

$$A = 2 \pi \lambda_0^2 g \Gamma_n \Gamma_\gamma / \Gamma \quad (2)$$

where  $\lambda_0$  is the neutron wave length of resonance,  $g$  the statistical spin factor and  $\Gamma_n$ ,  $\Gamma_\gamma$ ,  $\Gamma$  the neutron, gamma, and total width, respectively.

This result is essentially independent of resolution. Although the samples in the present experiments were thin as far as capture is concerned they are not thin for scattering, particularly in the large s-wave resonances. Therefore corrections must be made for multiple scattering and resonance self-protection effects. The corrections are carried out by a Monte Carlo calculation using the FORTRAN IV code, TACASI (16). When values of  $g$  and  $\Gamma_n$  are available from transmission measurements  $\Gamma_\gamma$  may be computed. Otherwise the analysis results in values of  $g \frac{\Gamma_n \Gamma_\gamma}{\Gamma}$ . The errors quoted for the radiation widths are of the order of 20 %. Tables 2-15 show the present resonance parameters.

#### 4. DISCUSSION

##### 4.1 The <sup>50, 52, 53</sup>Cr Nuclei

The present <sup>50</sup>Cr results for the neutron widths  $g\Gamma_n$  appear to be in good agreement with the results of Stieglitz et al. (17) whereas those of ref. (18) are somewhat different. For the neutron width of the <sup>50</sup>Cr (94.7 keV) resonance

we find a lower value which may be due to the direct inclusion of the broad  $^{52}\text{Cr}$  resonance nearby as a contaminant in our analysis. For  $^{52}\text{Cr}$  the present  $\Gamma_n$  results and those of ref. (17) and (18) are in fair agreement. It should be noted that the resonance near 140 keV in  $^{52}\text{Cr}$  was analyzed as a doublet in the present data. However, it can be fitted with  $\Gamma_n = 6.1$  keV, too, and this may be preferred. The  $^{52}\text{Cr}$  (31.62 keV) resonance is reported here as s-wave although within statistics of the data a higher l-wave shape would also fit.

The  $^{50,52,53}\text{Cr}$  radiation widths and  $g \frac{\Gamma_n \Gamma_\gamma}{\Gamma}$  values show in general good agreement with the values of ref. (17) except in the following points. The  $^{50}\text{Cr}$  (46.07 keV)  $l > 0$  wave resonance was not analyzed in ref. (17) although a resonance at that energy can be seen in their plot of the  $^{50}\text{Cr}$  capture yield per sample thickness. For the  $^{52}\text{Cr}$  (140 keV) resonance we found about half the radiation width compared to that of ref. (17). The difference may be partly due to the fact that in ref. (17) the resonance was analyzed with a larger  $\Gamma_n$  value. The radiation width of the  $^{52}\text{Cr}$  (96.2 keV) resonance was computed taking into account a  $l > 0$  wave resonance at 95.2 keV in contrast to ref. (17). Our value for the  $^{53}\text{Cr}$  (65.7 keV) total radiation width is about a factor of 4 larger than the radiation width of the s-wave resonance at 66.1 keV of ref. (17). In addition, in the present measurement the 65.7 keV s-wave resonance was found to be superimposed by  $l > 0$ -wave resonances at 62.1 and 64.1 keV whereas in ref. (17) only one  $l > 0$  wave resonance at 64.8 keV has been reported.

#### 4.2 The $^{54,57}\text{Fe}$ Nuclei

The  $^{54}\text{Fe}$  neutron widths of the 7.67, 52.78, and 71.80 keV resonances are in good agreement with results of ref. (19), (20), and (21). But some of the neutron widths of resonances at higher energies differ almost a factor of two with respect to ref. (19) and (20). These discrepancies can be the result of difficulties by the determination of the oxygen and hydrogen contaminants in ref. (20). No indication was found for a  $^{54}\text{Fe}$  (102 keV) resonance which was reported in (19) and was subsequently adopted by others. The  $l > 0$  wave  $^{54}\text{Fe}$  resonance at 11.2 keV was erroneously attributed to  $^{56}\text{Fe}$  by Hockenbury et al. (22).

The  $g \frac{\Gamma_n \Gamma_\gamma}{\Gamma}$  value of the  $^{54}\text{Fe}$  (14.44 keV) resonance of ref. (22) is in fair agreement with our radiation value. The present results for the radiation widths  $g \frac{\Gamma_n \Gamma_\gamma}{\Gamma}$  or  $\Gamma_\gamma$  of  $^{57}\text{Fe}$  are much smaller than the values reported by Macklin et al. (23) and Moxon (24). The discrepancies have probably their cause in the poorer energy resolution of the data in ref. (23) and (24). The  $g \frac{\Gamma_n \Gamma_\gamma}{\Gamma}$  and  $\Gamma_\gamma$  values of  $^{57}\text{Fe}$  reported in ref. (22) with some exceptions agree well with the present results.

#### 4.3 The $^{62,64}\text{Ni}$ Nuclei

For the isotopes  $^{62}\text{Ni}$  and  $^{64}\text{Ni}$  the present  $\Gamma_n$  values for s-wave resonances are in fair agreement with those of Farrell et al. (18) although our values appear to be systematically lower. The  $^{62}\text{Ni}$  (56.91 keV) resonance is clearly not s-wave as suggested in ref. (18). Garg et al. (21) give  $^{62}\text{Ni}$  resonance parameters which those authors have derived from transmission measurements on natural nickel samples. Our results on separated  $^{62}\text{Ni}$  samples clearly show that there is no resonance in  $^{62}\text{Ni}$  with a width as large as 0.25 keV near 89 keV neutron energy as obtained in (21). No radiation widths for  $^{62}\text{Ni}$  and  $^{64}\text{Ni}$  have been reported that can be compared with the present results.

### 5. STRENGTH FUNCTIONS

The s-wave strength functions derived from  $^{50,52}\text{Cr}$ ,  $^{54}\text{Fe}$  and  $^{62,64}\text{Ni}$  data are listed in Table 16. Values of other authors are included for comparison (17), (25). The present  $^{50,52}\text{Cr}$  values are in very good agreement with those reported in ref. (17). The high value for  $^{54}\text{Fe}$  is above the optical model calculations of Buck and Perey (26) as well as the doorway state calculations of Müller and Rohr (6).

With the assumption that the observed  $\ell > 0$  wave resonances may be considered as p-wave resonances the  $g \frac{\Gamma_n \Gamma_\gamma}{\Gamma}$  values can be used to calculate p-wave strength functions with the following equation according to ref. (17).

$$S_1 = \frac{1}{3\Delta E} \sum_{i=1}^N \frac{\langle g\Gamma_{ni} \rangle}{\sqrt{E_{oi}} v_i} \quad (3)$$

where  $\langle g\Gamma_{ni} \rangle$  is an estimated value for the  $i$ .th p-wave resonance,  $N$  is the number of p-wave resonance at energies  $E_{oi}$  in the energy range  $\Delta E$ .  $v_i$  is the penetrability factor

$$v_i = \frac{(k_{oi}R)^2}{1 + (k_{oi}R)^2} \quad (4)$$

with the neutron wave number  $k_{oi}$  and the potential scattering radius  $R$ . The calculation of the  $\langle g\Gamma_{ni} \rangle$  by means of the quantities  $g \frac{\Gamma_{ni}\Gamma_{\gamma i}}{\Gamma_i}$  is based on the assumption that the  $\Gamma_{\gamma i}$ 's can be regarded approximately as constant due to a chi-square distribution with high degree of freedom. The observed p-wave resonance widths in the transmission measurements give an upper limit for the  $\langle g\Gamma_{ni} \rangle$  values and therefore an estimate for the range of the  $g\Gamma_{\gamma i}$ 's. Our assumptions seem to be reasonable on the basis that the derived  $\Gamma_n^o$  values follow a Porter-Thomas distribution (Fig. 18). The error in the p-wave strength function is mainly due to the uncertainty in the  $g\Gamma_{\gamma}$  values. The strength function values for  $^{50,52,53}\text{Cr}$  are in agreement with values of ref. (17) (Table 17). The low p-wave strength functions reflect a predicted strength function minimum of  $0.2 \times 10^{-4}$  near mass 55 by Moldauer (27) and Jain (28).

## 6. NEUTRON WIDTH AND SPACING DISTRIBUTIONS

To check the consistency of our resonance parameters, the neutron width and spacing distributions were compared to Porter-Thomas and Wigner distributions, respectively. The reduced neutron widths for s-wave resonances of the even isotopes  $^{50,52}\text{Cr}$ ,  $^{54}\text{Fe}$ , and  $^{62,64}\text{Ni}$  were divided by their average reduced widths. A Porter-Thomas distribution of 61 levels appeared to give the best fit to the resulting distribution of 58 levels.

The neutron width distribution for p-waves was determined under the assumption that all analyzed  $l > 0$  wave resonances are p-wave resonances. The reduced neutron widths computation was carried out using the  $g \frac{\Gamma_{ni}\Gamma_{\gamma}}{\Gamma}$  values and an average  $g$  factor for each isotope similar to the p-wave strength function

calculation. The experimental distribution of 114 levels of all 7 isotopes were best fit by a Porter Thomas distribution of 160 levels (Fig. 18). Thus of the order of 46 levels were missed or not assigned as p-wave levels. The influence of d-wave levels was assumed to be small.

The differential distributions of resonance spacings of both the s- and p-wave resonances from  $^{50,52}\text{Cr}$ ,  $^{54}\text{Fe}$  and  $^{62,64}\text{Ni}$  are shown in Figures 19 along with the Wigner distribution. The spacing distribution of the p-wave resonances corresponds to a Wigner distribution of two populations (two spin states) (29). The inclusion of the missed levels would probably improve the already good agreement between experimentally observed distribution and Wigner distribution by introducing more smaller spacings.

## 7. CORRELATIONS

Nuclei in the region  $40 \leq A \leq 65$  have frequently been the object of searches for correlations in neutron capture in order to demonstrate the effects of particular initial or final state configurations on the transition probabilities for subsequent gamma-ray emission. Since for example the shell model  $2p_{3/2}$  and  $2p_{1/2}$  levels occur at relatively low excitation energies in these nuclei, and the  $3s_{1/2}$  and  $2d_{5/2}$  levels are expected at energies near the neutron separation energy, either direct capture or the valence neutron model reaction mechanism of Lynn (30) might contribute significantly to s-wave neutron capture. These processes would lead to enhanced high energy,  $E_1$  transitions to particular final states and to positive correlations in the capture results between the neutron reduced widths for s-wave resonances and the corresponding gamma-ray partial widths for transitions to a fixed final state. Jackson and Strait (31) and Baglan et al. (32) have obtained partial radiation widths for the ground state transitions of resonances in some of these nuclei from photonuclear reactions. To obtain partial radiation widths for the other transitions at each s-wave resonance is experimentally quite difficult for the nuclei in this mass region. However, it seems reasonable that if partial radiation widths - reduced neutron widths correlations do exist then also correlations might be expected to

occur between the neutron reduced widths for resonances and the corresponding total gamma-ray widths. Some mathematical basis for this assumption has been presented by Lane (33). Thus, Stieglitz et al. (17) have surveyed the resonance parameters of 27 s-wave resonances derived from their transmission and capture cross section measurements and have reported a strong positive correlation coefficient between neutron and total gamma-ray widths for the case of 12 resonances in some even-even target nuclei of Cr and Ni. As a result it is of interest to examine this region of nuclei in greater detail to establish the correlation with greater statistical accuracy and, even more important, to establish which individual nuclei show this effect. Therefore we have accumulated the results of a number of experimenters at the Karlsruhe 3 MV Van de Graaff (1) - (9) including the present measurements in order to establish with greater statistical accuracy the existence of neutron reduced width - total capture width correlations for nuclei in this mass region.

Joint correlation coefficients between  $\Gamma_\gamma$  and  $\Gamma_n^o$  were calculated for each spin state in each isotope separately. Then all the even isotopes were grouped together and all the odd isotopes were grouped together. Finally a correlation coefficient was computed for all isotopes. Eighty s-wave resonances in 12 nuclei were used in the analysis. The coefficients were calculated from the following expression:

$$\rho(\Gamma_\gamma, \Gamma_n^o) = \frac{\lambda \sum_{\lambda=1}^N (\Gamma_{\gamma\lambda} - \bar{\Gamma}_\gamma) (\Gamma_{n\lambda}^o - \bar{\Gamma}_n^o)}{\left\{ \sum_{\lambda=1}^N (\Gamma_{\gamma\lambda} - \bar{\Gamma}_\gamma)^2 \sum_{\lambda=1}^N (\Gamma_{n\lambda}^o - \bar{\Gamma}_n^o)^2 \right\}^{1/2}} \quad (5)$$

where  $\Gamma_{n\lambda}^o$  means the reduced neutron width of the  $\lambda$ -th resonance,  $\Gamma_{\gamma\lambda}$  the total radiation width of the  $\lambda$ -th resonance and N the number of resonances.

The results of these calculations are presented in Table 18. The errors quoted include uncertainties of the individual widths and the effect of finite sample size. In the cases where resonances in different isotopes have been grouped together the neutron and radiation widths for each isotope were individually normalized by dividing by their respective averages. The statistical significance P of the coefficients (last column in Table 18) has been estimated as follows :

Neutron reduced widths were chosen from a chi-square distribution with one degree of freedom and radiation widths were chosen from a chi-square distribution with six degrees of freedom (the six degrees of freedom are a lower limit of maximum likelihood estimates for the individual nuclei). This selection was done for the sample size of each individual isotope and for the sample size of each of the various groupings in Table 18. Correlation coefficients were then calculated from these simulated parameters. The procedure was repeated at least 10 000 times. The P values in Table 18 represent the fractional number of correlation coefficients so obtained which exceeded the lower limit of the experimentally determined value in each case.

The present analysis made use of 80 s-wave resonances in 12 nuclei in the mass region  $40 < A \leq 64$ . This represents a marked improvement in statistical accuracy compared to that available in reference (17). Similar to reference (17) a positive correlation greater than the 95 % confidence level was obtained for resonances in the even-even nuclei, but with a much reduced value of the correlation coefficient ( $\rho = 0.45$  compared to the  $\rho = 0.8$  of the above reference). Further, the present analysis shows a positive correlation at approximately the 95 % confidence level for the even-even isotope,  $^{60}\text{Ni}$ , and for the odd isotope,  $^{53}\text{Cr}$ . Closer examination of the parameters involved in the  $^{60}\text{Ni}$  case reveal that the observed correlation is due entirely to the single resonance at 12.5 keV ( $\rho$  for  $^{60}\text{Ni}$  is reduced to 0.024 for the eight remaining resonances, and, in addition,  $\rho$  for the even-even nuclei as a group reduces to 0.24).

Recently Jackson (34) found for  $^{52}\text{Cr}$  and  $^{60}\text{Ni}$  correlations between the reduced neutron widths and the partial radiation widths of ground state transitions. He obtained a correlation coefficient of 0.8 in the  $^{60}\text{Ni}$  case. This result indicates that our observed correlation in  $^{60}\text{Ni}$  is caused by the ground state transition of the 12.5 keV resonance.

From consideration of the sizes of the reduced neutron width and radiation width of the  $^{50}\text{Cr}$  5.6 keV resonance of ref. (17) which was not included in the present analysis, it is clear that this resonance also must have had a pronounced effect on the positive correlation reported in that reference (17).

Examination of the individual parameters in the case of  $^{53}\text{Cr}$  indicates that the positive correlation obtained here is due to several resonances, rather than a single broad resonance.

In conclusion, out of a large number of resonances in the mass region  $40 < A \leq 64$  significant positive correlations between neutron reduced widths and total radiation widths have been established for the low keV resonances in both  $^{60}\text{Ni}$  and  $^{53}\text{Cr}$ . These may be due to channel capture or intermediate structure effects in the capture mechanism of these two isotopes.

The authors would like to express their appreciation for the high purity separated isotopes which were made available through the USAEC-EANDC loan pool. We thank A. Ernst for his advice setting up the electronics of the tank. The help of the KFK Van de Graaff operating staff is also appreciated.

## REFERENCES

- (1) G. ROHR, E. FRIEDLAND, J. NEBE, Proc. Int. Conf. on nuclear data for reactors, Vol. I, Paris 1966 (IAEA, Vienna, 1967), p. 137 and Kernforschungszentrum Karlsruhe report KFK 452 (1966).
- (2) G. ROHR, E. FRIEDLAND, Nucl. Phys. A 104 (1967) 1.
- (3) G. ROHR, K.-N. MÜLLER, Z. Phys. 227 (1969) 1 and Kernforschungszentrum Karlsruhe report KFK 1072 (1969).
- (4) M. CHO, F.H. FRÖHNER, M. KAZEROUNI, K.-N. MÜLLER and G. ROHR, Proc. Int. Conf. on nuclear data for reactors, Vol. I, Helsinki 1970 (IAEA Vienna, 1970) p. 619 and Kernforschungszentrum Karlsruhe, report KFK 1230 (1970).
- (5) A. ERNST, D. KOMPE and F.H. FRÖHNER, Proc. Int. Conf. on nuclear data for reactors, Vol. I, Helsinki 1970 (IAEA, Vienna, 1970), p. 633 and Kernforschungszentrum Karlsruhe report KFK 1231 (1970).
- (6) K.-N. MÜLLER, G. ROHR, Nucl. Phys. A 164 (1971) 97 and Kernforschungszentrum Karlsruhe report KFK 1114 (1969).
- (7) R.R. SPENCER, H. BEER and F.H. FRÖHNER, Kernforschungszentrum Karlsruhe report KFK 1517, EANDC(E) 145 "AL" (1972).
- (8) H. BEER, R.R. SPENCER, F.H. FRÖHNER, M. CHO, Kernforschungszentrum Karlsruhe report KFK 1516, EANDC(E) 145 "AL" (1972).
- (9) F.H. FRÖHNER, Specialist's Panel on capture cross sections of structural materials, Karlsruhe 1973 (to be published).
- (10) H. BEER, 1971 (not published).
- (11) D. KOMPE, Nucl. Phys. A 133 (1969) 513.
- (12) E. SCHNEIDER, 1971 (not published).
- (13) A.M. LANE and R.G. THOMAS, Rev. Mod. Phys. 30 (1958) 257.
- (14) F.H. FRÖHNER, 1971 (not published).
- (15) F.P. MOORING, J.E. MONAHAM and C.M. HUDDLESTON, Nucl. Phys. 82 (1966) 16.
- (16) F.H. FRÖHNER, General Atomic report GA-6906 (1965).
- (17) R.G. STIEGLITZ, R.W. HOCKENBURY and R.C. BLOCK, Nucl. Phys. A 163 (1971) 592.
- (18) J.A. FARRELL, E.G. BILPUCH, H.W. NEWSON, Annals of Physics 37 (1966) 367.

- (19) H.W. NEWSON, E.G. BILPUCH, F.P. KARRIKER, L.W. WESTON, J.R. PATTERSON, C.D. BOWMAN, *Annals of Physics* 14 (1961) 365.
- (20) C.D. BOWMAN, E.G. BILPUCH, H.W. NEWSON, *Annals of Physics* 17 (1962) 319.
- (21) J.B. GARG, J. RAINWATER and W.W. HAVENS, jr., *Phys. Rev.* C3 (1971) 2447.
- (22) R.W. HOCKENBURY, R.M. BARTOLOME, J.R. TARTARCZUK, W.R. MAYER and R.C. BLOCK, *Phys. Rev.* 178 (1969) 1746.
- (23) R.L. MACKLIN, P.J. PASMA, J.H. GIBBONS, *Phys. Rev.* 136 (1964) B 695.
- (24) M.C. MOXON, *Int. Conf. on the study of nuclear structure with neutrons, Antwerp 1965*, paper 88.
- (25) K.K. SETH, *Nucl. Data Sect.* A2 (1966) 299.
- (26) B. BUCK and F. PEREY, *Phys. Rev. Lett.* 8 (1962) 444.
- (27) P. MOLDAUER, *Nucl. Phys.* 47 (1963) 65.
- (28) A.P. JAIN, *Nucl. Phys.* 50 (1964) 157.
- (29) J.A. HARVEY and D.J. HUGHES, *Phys. Rev.* 109 (1958) 471.
- (30) J.E. LYNN, *The theory of neutron resonance reactions* (Clarendon Press, Oxford, England, 1968).
- (31) H.E. JACKSON and E.N. STRAIT, *Phys. Rev.* C4 (1971) 1314.
- (32) R.J. BAGLAN, C.D. BOWMAN and B.L. BERMAN, *Phys. Rev.* C3 (1971) 2475.
- (33) A.M. LANE, *Proc. Int. Symposium on neutron  $\gamma$ -ray spectr., Studsvik 1969 (IAEA, Vienna, 1969) p. 513.*
- (34) H.E. JACKSON, *Threshold Photoneutron Spectra, 2nd Int. Symp. on neutron capture  $\gamma$ -ray Spectr., Petten 1974 (to be published).*

TABLE 1 Sample characteristics

transmission		capture		Isotopic composition (atomic fraction)				
g	at/b	g	at/b					
		$\text{Cr}_2\text{O}_3$		$^{50}\text{Cr}$	$^{52}\text{Cr}$	$^{53}\text{Cr}$	$^{54}\text{Cr}$	
6.90	0.126	43.75	0.018	0.9680	0.0298	0.0018	0.0004	
4.02	0.073							
13.05	0.232	81.45	0.032	0.0002	0.9974	0.0023	0.0001	
7.96	0.142							
-		36.51	0.014	<0.0005	0.0344	0.9640	0.0018	
		$\text{Fe}_2\text{O}_3$		$^{54}\text{Fe}$	$^{56}\text{Fe}$	$^{57}\text{Fe}$	$^{58}\text{Fe}$	
5.98	0.102							
2.11	0.036	68.57	0.026	0.9769	0.0225	0.0005	0.0001	
9.22	0.157							
3.91	0.067							
-		40.34	0.015	0.0012	0.0643	0.9236	0.0009	
		Ni		$^{58}\text{Ni}$	$^{60}\text{Ni}$	$^{61}\text{Ni}$	$^{62}\text{Ni}$	$^{64}\text{Ni}$
8.49	0.073	24.82	0.0047	0.0047	0.0056	0.0022	0.9875	<0.0005
5.07	0.044							
10.63	0.089	11.98	0.0070	0.0092	0.0073	0.0005	0.0038	0.9792
4.24	0.035							

<sup>+</sup> Samples were obtained through the USAEC-EANDC loan pool.

TABLE 2

The s-wave resonances of  $^{50}\text{Cr}$ 

$E_0$ (keV)	$\Gamma_n$ (keV)	$\Gamma_\gamma$ (eV)	% Multiple Scattering
$28.43 \pm 0.09$	$0.415 \pm 0.010$	$0.47 \pm 0.09$	10
$37.32 \pm 0.12$	$2.24 \pm 0.03$	$1.97 \pm 0.30$	25
$54.99 \pm 0.18$	$0.281 \pm 0.017$	$0.69 \pm 0.13$	2
$64.8 \pm 0.2$	$0.043 \pm 0.020$		
$94.75 \pm 0.4$	$1.67 \pm 0.05$	$0.65 \pm 0.14$	6
$114.8 \pm 0.5$	$0.12 \pm 0.05$		
$129.0 \pm 0.6$	$0.54 \pm 0.08$	$1.48 \pm 0.30$	2
$156.6 \pm 0.7$	$1.23 \pm 0.11$		
$162.45 \pm 0.8$	$0.75 \pm 0.10$		
$185.2 \pm 0.9$	$3.52 \pm 0.14$		
$218.3 \pm 1.2$	$0.17 \pm 0.13$		
$231.6 \pm 1.2$	$0.94 \pm 0.15$		
$245.6 \pm 1.4$	$0.20 \pm 0.15$		
$276.6 \pm 1.5$	$1.9 \pm 0.2$		
289.8	3.7		

 $E_n < 117 \text{ keV}$  $E_n > 117 \text{ keV}$  $a_J = 4.7 \text{ fm}$  $a_J = 4.2 \text{ fm}$  $S_J^1 = 0$  $S_J^1 = 4 \times 10^{-4}$

TABLE 3

The  $\ell > 0$  resonances of  $^{50}\text{Cr}$ 

$E_o$ (keV)	$g_n^\Gamma$ (keV)	$g_n^\Gamma \Gamma_\gamma / \Gamma$ (eV)	$g_\gamma^\Gamma$ (eV)
18.60 $\pm$ 0.07		0.57 $\pm$ 0.09	
19.18 $\pm$ 0.07		0.46 $\pm$ 0.08	
24.08 $\pm$ 0.10		0.08 $\pm$ 0.02	
24.84 $\pm$ 0.11		0.31 $\pm$ 0.06	
33.45 $\pm$ 0.18		0.85 $\pm$ 0.12	
35.4 $\pm$ 0.2		1.51 $\pm$ 0.21	
40.6 $\pm$ 0.2		0.86 $\pm$ 0.13	
46.7 $\pm$ 0.3		0.69 $\pm$ 0.10	
50.0 $\pm$ 0.3		0.56 $\pm$ 0.10	
53.4 $\pm$ 0.3		0.68 $\pm$ 0.12	
59.1 $\pm$ 0.4		1.05 $\pm$ 0.16	
63.5 $\pm$ 0.4			
65.6 $\pm$ 0.5			
70.2 $\pm$ 0.5			

TABLE 4      The s-wave resonances of  $^{52}\text{Cr}$

$E_0$ (keV)	$\Gamma_n$ (keV)	$\Gamma_\gamma$ (eV)	% Multiple Scattering
$31.62 \pm 0.10$	$0.015 \pm 0.008$	$0.26 \pm 0.14$	2
$50.19 \pm 0.16$	$1.71 \pm 0.02$	$1.0 \pm 0.15$	26
$96.2 \pm 0.4$	$6.40 \pm 0.06$	$4.0 \pm 0.5$	30
$118.1 \pm 0.5$	$\approx 0.03$		
$121.4 \pm 0.5$	$0.61 \pm 0.06$	$1.5 \pm 0.2$	6
$140.0 \pm 0.6$	$6.1 \pm 0.2$	$1.1 \pm 0.2$	18
$249.3 \pm 1.4$	$0.55 \pm 0.16$		

$$E_n < 90 \text{ keV}$$

$$a_J = 4.5 \text{ fm}$$

$$S'_J = 1.5 \times 10^{-4}$$

$$E_n > 90 \text{ keV}$$

$$a_J = 4.4 \text{ fm}$$

$$S'_J = 3 \times 10^{-4}$$

TABLE 5

The  $\ell > 0$  resonances of  $^{52}\text{Cr}$ 

$E_0$ (keV)	$g\Gamma_n$ (keV)	$g\Gamma_n \Gamma_\gamma / \Gamma$ (eV)	$g\Gamma_\gamma$ (eV)
$22.92 \pm 0.07$	$\approx 0.005$	$0.44 \pm 0.06$	$\approx 0.48$
<b>27.6</b> $\pm 0.13$		$0.39 \pm 0.05$	
$34.0 \pm 0.2$		$0.26 \pm 0.04$	
$48.2 \pm 0.3$		$0.70 \pm 0.09$	
$57.6 \pm 0.2$	$0.079 \pm 0.017$	$0.50 \pm 0.08$	$0.50 \pm 0.12$
$78.9 \pm 0.6$		$0.39 \pm 0.06$	
$95.2 \pm 1.0$		$0.78 \pm 0.15$	
$106.0 \pm 0.4$	$0.06 \pm 0.04$		
$111.6 \pm 0.5$	$0.06 \pm 0.05$		
$\approx 113$			
$130.1 \pm 0.6$	$0.22 \pm 0.06$	$1.34 \pm 0.20$	$1.35 \pm 0.5$
$153.3 \pm 1.7$		$0.77 \pm 0.16$	
$165.3 \pm 2.0$			
$234.0 \pm 1.3$	$0.3 \pm 0.2$		
$235.8 \pm 1.3$	$1.1 \pm 0.2$		
$242.6 \pm 1.4$	$0.22 \pm 0.15$		
$246.3 \pm 1.4$	$1.01 \pm 0.16$		
$256.7 \pm 1.5$	$0.31 \pm 0.17$		
$281.9 \pm 1.6$	$0.55 \pm 0.19$		

TABLE 6      The s-wave resonances of  $^{53}\text{Cr}$

$E_0$ (keV)	J	$\Gamma_n$ (keV)	$\Gamma_\gamma$ (eV)	% Multiple Scattering
8.18	2	$1.03 \pm 0.09^{+)}$	$3.2 \pm 0.3$	105
19.53	2	$0.13 \pm 0.02$	$0.8 \pm 0.1$	4
25.64	2	$0.22 \pm 0.03$	$0.7 \pm 0.1$	5
26.95	1	$0.70 \pm 0.10$	$1.6 \pm 0.1$	10
29.23	2	$0.33 \pm 0.03$	$0.9 \pm 0.1$	5
65.7	2	$4.5 \pm 0.07$	$3.1 \pm 0.3$	11
73.1	1	$1.05 \pm 0.25$	$2.5 \pm 0.3$	8
74.06	2	$1.2 \pm 0.2$	$2.0 \pm 0.3$	9
87.2	1	$7.8 \pm 1.0$	$4.5 \pm 0.6$	10
94.5	2	$0.6 \pm 0.1$		
99.7	1	$0.4 \pm 0.1$		
107.4	2	$1.5 \pm 0.15$	$3.2 \pm 0.3$	3
123.6	1	$4.0 \pm 1.0$		
124.5	2	$0.5 \pm 0.2$		
127.6	2	$0.4 \pm 0.2$		
129.5	2	$0.2 \pm 0.1$		
135.0	1	$24.0 \pm 5.0$		
145.9	2	$0.6 \pm 0.1$		
157.8	2	$0.9 \pm 0.1$		
159.0	2	$2.0 \pm 0.3$		
172.7	2	$1.2 \pm 0.2$		
175.7	1	$4.0 \pm 0.8$		
183.0	1	$3.5 \pm 0.7$		
186.0	2	$0.5 \pm 0.2$		
195.7	2	$0.6 \pm 0.1$		
201.7	2	$0.55 \pm 0.1$		
221.6	2	$4.2 \pm 0.8$		
227.5	2	$0.3 \pm 0.1$		
239.0	2	$3.0 \pm 0.6$		
244.5	1	$4.0 \pm 1.0$		
246.0	2	$0.5 \pm 0.3$		

+ ) Stieglitz et al. (17)

TABLE 7

The  $\ell > 0$  resonances of  $^{53}\text{Cr}$ 

$E_0$ (keV)	$g\Gamma_n$ (keV)	$g\Gamma_n\Gamma_\gamma / \Gamma$ (eV)	$g\Gamma_\gamma$ (eV)
12.12 ± 0.08		0.17 ± 0.04	
20.15 ± 0.08		0.47 ± 0.05	
21.16 ± 0.08		0.09 ± 0.03	
22.35 ± 0.09		0.23 ± 0.04	
25.61 ± 0.12		0.028 ± 0.005	
28.70 ± 0.13		0.64 ± 0.05	
31.46 ± 0.15		0.28 ± 0.03	
31.94 ± 0.15		0.26 ± 0.03	
34.9 ± 0.2		0.27 ± 0.03	
37.6 ± 0.2		0.26 ± 0.03	
42.2 ± 0.2		0.31 ± 0.04	
43.0 ± 0.3		0.29 ± 0.04	
46.70 ± 0.07	≈0.02	0.45 ± 0.05	≈0.46
49.6 ± 0.3		0.27 ± 0.04	
50.70 ± 0.08	≈0.03	0.16 ± 0.05	≈0.16
53.2 ± 0.3		0.56 ± 0.08	
62.1 ± 0.4		0.64 ± 0.06	
64.1 ± 0.5		0.50 ± 0.05	
69.25 ± 0.13	≈0.03	1.10 ± 0.11	≈1.14
84.9 ± 0.7		1.04 ± 0.11	
88.7 ± 0.7		0.70 ± 0.08	
93.6 ± 0.2	≈0.04	1.15 ± 0.23	≈1.18
97.81 ± 0.2	≈0.02		
98.98 ± 0.2	≈0.03		
103.87 ± 0.2	≈0.04		
105.50 ± 0.2	≈0.04		

TABLE 8

The s-wave resonances of  $^{54}\text{Fe}$ 

$E_0$ (keV)	$\Gamma_n$ (keV)	$\Gamma_\gamma$ (eV)	% Multiple Scattering
$7.67 \pm 0.02$	$1.01 \pm 0.01$		
$52.78 \pm 0.18$	$2.16 \pm 0.02$	$1.8 \pm 0.3$	23
$71.86 \pm 0.25$	$1.77 \pm 0.03$	$0.8 \pm 0.2$	12
$98.5 \pm 0.4$	$0.51 \pm 0.05$	$3.2 \pm 0.5$	11
$129.6 \pm 0.5$	$3.00 \pm 0.09$	$3.0 \pm 0.6$	9
$147.1 \pm 0.7$	$2.75 \pm 0.11$	$3.0 \pm 0.6$	5
$159.0 \pm 0.8$	$0.18 \pm 0.09$	$3.9 \pm 0.8$	1
$173.9 \pm 0.8$	$2.8 \pm 0.1$	$2.4 \pm 0.5$	2
$191.2 \pm 1.0$	$42.4 \pm 0.5$		
$222.8 \pm 1.2$	$1.57 \pm 0.14$		
$230.2 \pm 1.2$	$0.26 \pm 0.14$		
$245.7 \pm 1.3$	$24.6 \pm 0.6$		

$$E_n < 22 \text{ keV}$$

$$a_J = 4.0 \text{ fm}$$

$$S_J^1 = 11.7 \times 10^{-4}$$

$$22 \text{ keV} < E_n < 90 \text{ keV}$$

$$a_J = 3.8 \text{ fm}$$

$$S_J^1 = 13 \times 10^{-4}$$

$$E_n < 90 \text{ keV}$$

$$a_J = 4.27 \text{ fm}$$

$$S_J^1 = 11.2 \times 10^{-4}$$

TABLE 9

The  $\ell > 0$  resonances of  $^{54}\text{Fe}$ 

$E_0$ (keV)	$g\Gamma_n$ (keV)	$g\Gamma_n \Gamma_\gamma / \Gamma$ (eV)	$g\Gamma_\gamma$ (eV)
11.19 ± 0.03	≈0.007	0.80 ± 0.16	≈0.9
14.44 ± 0.08		0.92 ± 0.16	
22.97 ± 0.16		0.57 ± 0.11	
28.24 ± 0.10		0.16 ± 0.06	
30.70 ± 0.10	≈0.010	1.07 ± 0.16	≈1.2
35.31 ± 0.15		0.33 ± 0.07	
38.5 ± 0.2		1.00 ± 0.15	
39.18 ± 0.12	≈0.015	1.31 ± 0.19	≈1.4
51.7 ± 0.3		0.40 ± 0.08	
53.7 ± 0.4		0.76 ± 0.11	
55.46 ± 0.19	0.03 ± 0.02	0.90 ± 0.13	0.9 ± 0.7
59.3 ± 0.3		0.46 ± 0.08	
68.8 ± 0.4		0.5 ± 0.1	
75.9 ± 0.5		1.0 ± 0.2	
77.4 ± 0.5		1.5 ± 0.3	
83.4 ± 0.5		≈1.7	
87.4 ± 0.6		0.8 ± 0.2	
104.3 ± 1.0		1.1 ± 0.2	
113.0 ± 0.8		1.5 ± 0.3	
115.7 ± 0.8		1.3 ± 0.2	
120.3 ± 0.8		2.6 ± 0.4	
126.3 ± 1.0		2.3 ± 0.3	
142.4 ± 1.2			
152 ± 2			
165 ± 1.5			

TABLE 10 The s-wave resonances of  $^{57}\text{Fe}$

$E_0$ (keV)	J	$\Gamma_n$ (keV)	$\Gamma_n'$ (keV)	$\Gamma_\gamma$ (eV)	% Multiple Scattering
29.15	1	$3.45 \pm 0.4$	$1.0 \pm 0.1$	$2.3 \pm 0.3$	36
41.40	1	$1.0 \pm 0.1$	$2.55 \pm 0.3$	$0.9 \pm 0.2$	22
47.05	1	$0.45 \pm 0.1$	<0.05	$0.55 \pm 0.05$	3
55.81	0	$10.0 \pm 1.5$			
61.0	1	$3.7 \pm 0.5$	$0.3 \pm 0.1$	$1.2 \pm 0.1$	17
77.2	1	$1.95 \pm 0.2$	$0.75 \pm 0.1$	$0.5 \pm 0.1$	7
93.7	1	$0.2 \pm 0.05$	$0.2 \pm 0.05$	$1.9 \pm 0.2$	4
109.6	1	$2.3 \pm 0.3$	<0.2		
110.15	1	$1.2 \pm 0.1$	$1.55 \pm 0.2$	$2.0 \pm 0.3$	6
125.0	1	$1.5 \pm 0.2$	$1.0 \pm 0.1$		
126.0	0	$2.5 \pm 0.5$			
129.5	1	$4.2 \pm 0.7$	$8.0 \pm 1.0$		
134.5	0	$3.3 \pm 0.5$			
141.0	0	$1.5 \pm 0.3$			
167.3	1	$1.1 \pm 0.1$	$0.9 \pm 0.1$		
169.0	1	$1.7 \pm 0.2$	$1.2 \pm 0.15$		
176.3	0	$0.7 \pm 0.1$			
185.5	1	$3.5 \pm 0.4$	<0.4		
189.5	0	$3.2 \pm 0.4$			

TABLE 11

The  $\ell > 0$  resonances of  $^{57}\text{Fe}$ 

$E_0$ (keV)	$g\Gamma_n$ (keV)	$g\Gamma_n \Gamma_\gamma / \Gamma$ (eV)	$g\Gamma_\gamma$ (eV)
7.17 ± 0.03		0.42 ± 0.08	
7.87 ± 0.04		0.25 ± 0.05	
12.73 ± 0.08		0.27 ± 0.02	
13.93 ± 0.09		0.40 ± 0.06	
18.25 ± 0.02	≈0.004	0.47 ± 0.04	≈0.54
21.28 ± 0.03	≈0.003	0.60 ± 0.05	≈0.74
24.85 ± 0.11		0.08 ± 0.02	
25.79 ± 0.12		0.05 ± 0.02	
27.23 ± 0.12		0.06 ± 0.02	
28.64 ± 0.13		0.29 ± 0.03	
31.94 ± 0.16		0.17 ± 0.02	
35.18 ± 0.18		0.35 ± 0.04	
37.01 ± 0.06	≈0.004	0.27 ± 0.02	≈0.29
39.36 ± 0.06	≈0.008	0.41 ± 0.04	≈0.43
41.93 ± 0.07	≈0.004	0.16 ± 0.03	≈0.17
51.1 ± 0.3		0.12 ± 0.02	
52.66 ± 0.10	≈0.016	0.33 ± 0.05	≈0.34
56.20 ± 0.11	≈0.003	0.14 ± 0.03	≈0.15
58.7 ± 0.4		0.08 ± 0.03	
64.0 ± 0.5		0.39 ± 0.04	
66.8 ± 0.5		0.36 ± 0.04	
72.9 ± 0.6		0.28 ± 0.04	
80.7 ± 0.6		0.32 ± 0.04	
88.0 ± 0.2	≈0.019		
89.7 ± 0.2	≈0.015		
101.8 ± 0.3	≈0.013	0.53 ± 0.05	≈0.56
119.2 ± 0.4	≈0.021		

TABLE 12

The s-wave resonances of  $^{62}\text{Ni}$ 

$E_o$ (keV)	$\Gamma_n$ (keV)	$\Gamma_\gamma$ (eV)	% Multiple Scattering
42.87 $\pm$ 0.14	0.340 $\pm$ 0.015	0.36 $\pm$ 0.07	4
77.2 $\pm$ 0.3	0.07 $\pm$ 0.03		
94.7 $\pm$ 0.4	2.5 $\pm$ 0.1	0.56 $\pm$ 0.13	6
105.6 $\pm$ 0.4	4.6 $\pm$ 0.2	1.40 $\pm$ 0.31	12
149.3 $\pm$ 0.7	0.14 $\pm$ 0.07		
188.2 $\pm$ 0.9	$\approx$ 0.09		
214.7 $\pm$ 1.1	0.19 $\pm$ 0.13		
229.5 $\pm$ 1.2	6.18 $\pm$ 0.16		
243.2 $\pm$ 1.3	0.78 $\pm$ 0.15		
281.1 $\pm$ 1.6	4.8 $\pm$ 0.4		
$\approx$ 288.0	$\approx$ 1.0		

$E_n < 90$  keV

$a_J = 6.0$  fm

$S'_J = 7.8 \times 10^{-4}$

$E_n > 90$  keV

$a_J = 6.5$  fm

$S'_J = 4.1 \times 10^{-4}$

TABLE 13

The  $\ell > 0$  resonances of  $^{62}\text{Ni}$ 

$E_0$ (keV)	$g\Gamma_n$ (keV)	$g\Gamma_n \Gamma_\gamma / \Gamma$ (eV)	$g\Gamma_\gamma$ (eV)
8.91 ± 0.10		0.082 ± 0.016	
9.42 ± 0.10		0.24 ± 0.04	
17.69 ± 0.07		0.13 ± 0.03	
24.46 ± 0.11		0.17 ± 0.03	
28.22 ± 0.14		0.26 ± 0.04	
29.29 ± 0.14		0.50 ± 0.07	
34.28 ± 0.18		0.36 ± 0.06	
38.04 ± 0.20		0.77 ± 0.11	
40.3 ± 0.3		0.12 ± 0.03	
41.0 ± 0.3		0.19 ± 0.04	
44.8 ± 0.3		0.34 ± 0.07	
53.1 ± 0.3		0.15 ± 0.05	
56.91 ± 0.19	0.056 ± 0.017	0.28 ± 0.07	0.28 ± 0.11
63.1 ± 0.4		0.27 ± 0.07	
74.0 ± 0.5		0.47 ± 0.09	
78.4 ± 0.3		0.14 ± 0.04	
93.4 ± 0.8		0.55 ± 0.12	
103.3 ± 0.8		1.30 ± 0.22	
112.0 ± 0.9		0.81 ± 0.20	
118.5 ± 1.1		1.52 ± 0.33	
137.4 ± 1.4		1.77 ± 0.44	
145.0 ± 1.5		3.09 ± 0.62	
160.5 ± 1.8		2.72 ± 0.60	

TABLE 14

The s-wave resonances of  $^{64}\text{Ni}$ 

$E_0$ (keV)	$\Gamma_n$ (keV)	$\Gamma_\gamma$ (eV)	% Multiple Scattering
14.3 $\pm$ 0.2	2.9 $\pm$ 0.5	1.9 $\pm$ 0.4	96
33.82 $\pm$ 0.10	8.90 $\pm$ 0.05	2.9 $\pm$ 0.6	52
129.3 $\pm$ 0.5	1.34 $\pm$ 0.07		
148.8 $\pm$ 0.7	0.08 $\pm$ 0.07		
155.0 $\pm$ 0.7	3.9 $\pm$ 0.1		
163.2 $\pm$ 0.8	0.14 $\pm$ 0.08		
177.7 $\pm$ 0.8	0.47 $\pm$ 0.09		
205.3 $\pm$ 1.1	$\approx$ 0.06		
219.8 $\pm$ 1.1	$\approx$ 0.03		
226.9 $\pm$ 1.2	$\approx$ 0.12		
231.9 $\pm$ 1.2	3.77 $\pm$ 0.16		
269.7 $\pm$ 1.5	2.2 $\pm$ 0.2		
283.5 $\pm$ 1.6	0.35 $\pm$ 0.19		

$$E_n < 98 \text{ keV}$$

$$a_J = 6.4 \text{ fm}$$

$$S'_J = 3.4 \times 10^{-4}$$

$$E_n > 98 \text{ keV}$$

$$a_J = 6.4 \text{ fm}$$

$$S'_J = 1.6 \times 10^{-4}$$

**TABLE 15**

The  $\ell > 0$  resonances of  $^{64}\text{Ni}$

$E_0$ (keV)	$g\Gamma_n$ (keV)	$g\Gamma_n\Gamma_\gamma/\Gamma$ (eV)
14.8 ± 0.1		0.24 ± 0.05
31.85 ± 0.15		0.75 ± 0.11
62.8 ± 0.4		0.85 ± 0.18
106.5 ± 0.4	0.11 ± 0.05	
142.0 ± 0.6	0.17 ± 0.07	
191.5 ± 0.9	0.16 ± 0.11	
214.7 ± 1.1	≈ 0.08	
237.9 ± 1.3	0.32 ± 0.13	
255.7 ± 1.4	0.17 ± 0.15	

TABLE 16 The s-wave neutron strength functions

Target nucleus	Experimental strength function	
	$(S_0 \times 10^{-4})$	
$^{50}\text{Cr}$	$1.7 \pm 0.7$	$2.18 \pm 0.75$ (17)
$^{52}\text{Cr}$	$1.9 \pm 1.0$	$2.10 \pm 1.05$ (17)
$^{54}\text{Fe}$	$7.8 \pm 3.4$	$5.2 \pm 1.7$ (25)
$^{62}\text{Ni}$	$1.8 \pm 0.9$	$2.9 \pm 0.8$ (25)
$^{64}\text{Ni}$	$3.5 \pm 1.4$	$2.0 \pm 0.7$ (25)

TABLE 17 The p-wave neutron strength functions

Target nucleus	Energy range (keV)	p-wave strength function $S_1 \times 10^{-4}$	
$^{50}\text{Cr}$	6 - 60	$0.36 \pm 0.27$	$0.264 \pm 0.152$ (17)
$^{52}\text{Cr}$	6 - 154	$0.068 \pm 0.060$	$0.053 \pm 0.023$ (17)
$^{53}\text{Cr}$	6 - 94	$0.081 \pm 0.051$	$0.074 \pm 0.050$ (17)
$^{54}\text{Fe}$	10 - 127	$0.18 \pm 0.08$	
$^{57}\text{Fe}$	6 - 102	$0.55 \pm 0.43$	
$^{62}\text{Ni}$	6 - 161	$0.028 \pm 0.013$	

Table 18. Correlation analysis

Element	J	Number of Resonances	$\rho(\Gamma_\gamma, \Gamma_n^0)$	P %
$^{47}\text{Ti}$	2	5	$+ 0.58 \pm 0.70$	76
	3	4	$- 0.20 \pm 0.83$	99
$^{50}\text{Cr}$	$\frac{1}{2}$	5	$+ 0.64 \pm 0.48$	30
$^{52}\text{Cr}$	$\frac{1}{2}$	5	$+ 0.74 \pm 0.53$	27
$^{53}\text{Cr}$	1	3	$+ 0.95 \pm 0.82$	41
	2	7	$+ 0.77 \pm 0.35$	12
$^{53}\text{Cr}^+)$	2	8	$+ 0.76 \pm 0.30$	9.2
$^{53}\text{Cr}^+)$	1,2	13	$+ 0.74 \pm 0.23$	3.2
$^{54}\text{Fe}$	$\frac{1}{2}$	7	$- 0.61 \pm 0.43$	43
$^{56}\text{Fe}$	$\frac{1}{2}$	4	$- 0.32 \pm 0.47$	61
$^{57}\text{Fe}$	1	7	$+ 0.28 \pm 0.32$	43
$^{58}\text{Ni}$	$\frac{1}{2}$	5	$- 0.46 \pm 0.81$	90
$^{60}\text{Ni}$	$\frac{1}{2}$	9	$+ 0.80 \pm 0.28$	5.7
$^{61}\text{Ni}$	1	7	$- 0.18 \pm 0.35$	71
	2	7	$- 0.09 \pm 0.42$	75
$^{62}\text{Ni}$	$\frac{1}{2}$	3	$+ 0.94 \pm 0.87$	28
$^{64}\text{Ni}$	$\frac{1}{2}$	2	$+ 1.00 \pm 1.18$	100
Sum:Even All	-	40	$+ 0.45 \pm 0.10$	1.6
Sum:Even $^{50}, ^{52}\text{Cr}$ $^{60}, ^{62}, ^{64}\text{Ni}$	-	24	$+ 0.70 \pm 0.15$	0.4
Sum:Odd All	-	40	$+ 0.30 \pm 0.13$	13
Sum:All	-	80	$+ 0.39 \pm 0.07$	0.4

+ ) including total radiation widths of ref. (17).

FIGURE CAPTIONS

Fig. 1 - 2 : (below) - The transmission data and R-matrix fit for the chromium-oxide samples, enriched in  $^{50}\text{Cr}$ , vs. neutron energy.

(middle) - Resolution broadened, total cross-section for the pure isotope  $^{50}\text{Cr}$  computed from the R-matrix parameters.

(above) -  $^{50}\text{Cr}$  capture yield divided by sample thickness vs. neutron energy.

Fig. 3 - 4 : (below) - The transmission data and R-matrix fit for the chromium-oxide samples, enriched in  $^{52}\text{Cr}$ , vs. neutron energy.

(middle) - Resolution broadened, total cross-section for the isotope  $^{52}\text{Cr}$  computed from the R-matrix parameters.

(above) -  $^{52}\text{Cr}$  capture yield divided by sample thickness vs. neutron energy.

Fig. 5 - 6 : (below) - The transmission data and R-matrix fit for the chromium-oxide samples, enriched in  $^{53}\text{Cr}$ , vs. neutron energy.

(middle) - Resolution broadened, total cross-section for the pure isotope  $^{53}\text{Cr}$  computed from the R-matrix parameters.

(above) -  $^{53}\text{Cr}$  capture yield divided by sample thickness vs. neutron energy.

Fig. 7 - 9 : (below) - The transmission data and R-matrix fit for the iron-oxide samples, enriched in  $^{54}\text{Fe}$ , vs. neutron energy.

(middle) - Resolution broadened, total cross-section for the pure isotope  $^{54}\text{Fe}$  computed from the R-matrix parameters.

(above) -  $^{54}\text{Fe}$  capture yield divided by sample thickness  
vs. neutron energy.

Fig. 10 - 12 : (below) - The transmission data and R-matrix fit for the  
iron-oxide samples, enriched in  $^{57}\text{Fe}$ , vs. neutron energy.

(middle) - Resolution broadened, total cross-section for the  
pure isotope  $^{57}\text{Fe}$  computer from the R-matrix parameters.

(above) -  $^{57}\text{Fe}$  capture yield divided by sample thickness  
vs. neutron energy.

Fig. 13 - 14 : (below) - The transmission data and R-matrix fit for the  
nickel samples, enriched in  $^{62}\text{Ni}$ , vs. neutron energy.

(middle) - Resolution broadened total cross-section for the  
pure  $^{62}\text{Ni}$  isotope computed from the R-matrix parameters.

(above) -  $^{62}\text{Ni}$  capture yield divided by sample thickness  
vs. neutron energy.

Fig. 15 : (below) - The transmission data and R-matrix fit for the  
nickel sample, enriched in  $^{64}\text{Ni}$ , vs. neutron energy in the  
region 16 - 98 keV.

(middle) - Resolution broadened, total cross-section for the  
pure isotope  $^{64}\text{Ni}$  computed from the R-matrix parameters.

(above) -  $^{64}\text{Ni}$  capture yield divided by sample thickness vs.  
neutron energy in the region 8 - 90 keV.

Fig. 16 : (below) - The transmission data and R-matrix fit for the  
nickel samples, enriched in  $^{64}\text{Ni}$ , vs. neutron energy, in the  
region 98- 290 keV.

(above) - Resolution broadened, total cross-section for the pure isotope  $^{64}\text{Ni}$  computed from the R-matrix parameters.

Fig. 17 : Integral distribution of reduced neutron widths for s-wave resonances of  $^{50, 52}\text{Cr}$ ,  $^{54}\text{Fe}$ , and  $^{62, 64}\text{Ni}$ .

Fig. 18 : Integral distribution of reduced neutron widths for p-wave resonances of  $^{50, 52, 53}\text{Cr}$ ,  $^{54, 57}\text{Fe}$ , and  $^{62, 64}\text{Ni}$ .

Fig. 19 : Differential distribution of the p-wave resonance level spacings (below) and the s-wave resonance level spacings (above) of  $^{50, 52}\text{Cr}$ ,  $^{54}\text{Fe}$ , and  $^{62, 64}\text{Ni}$ .

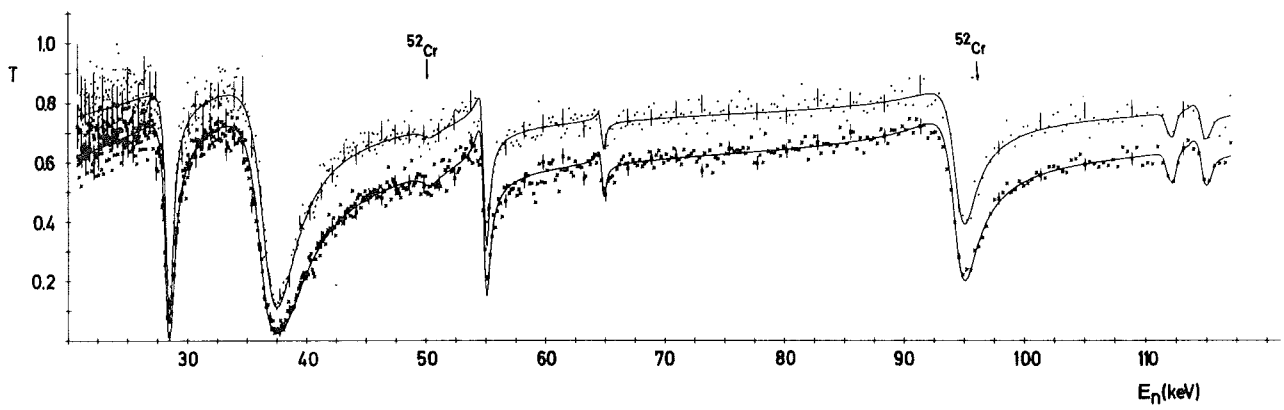
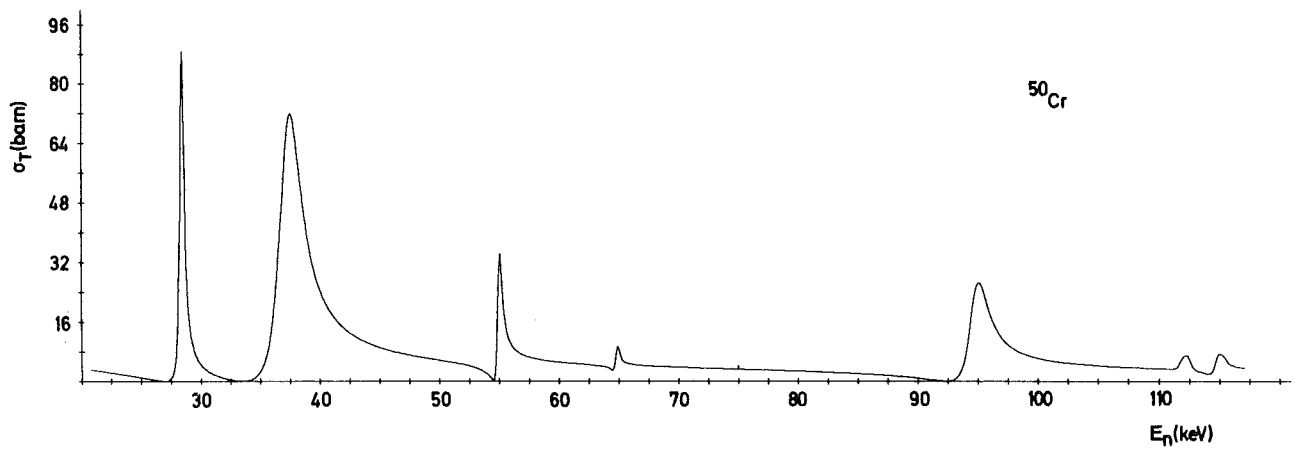
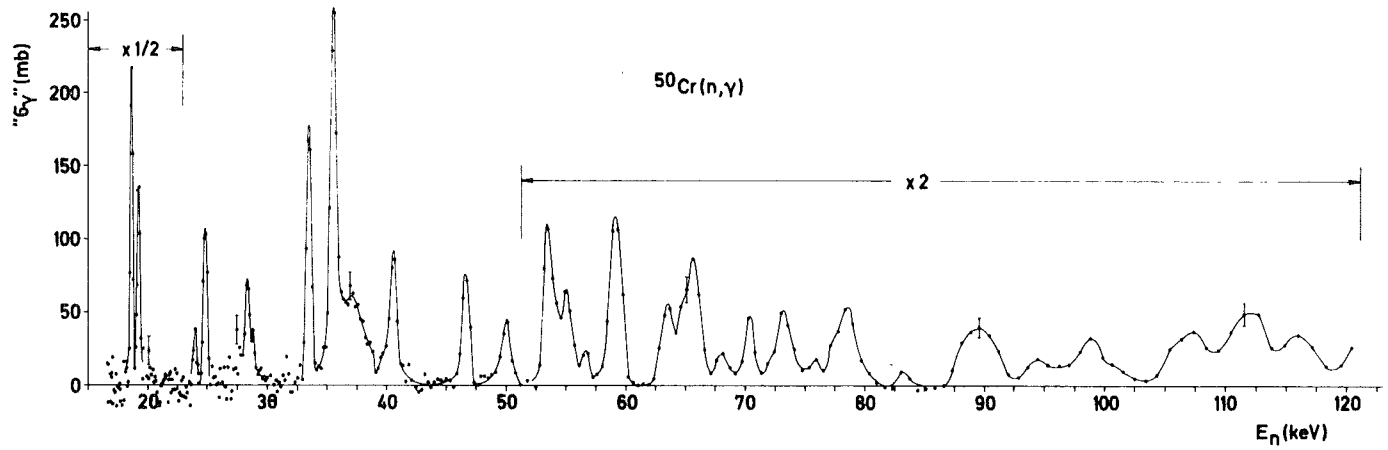


Fig.1

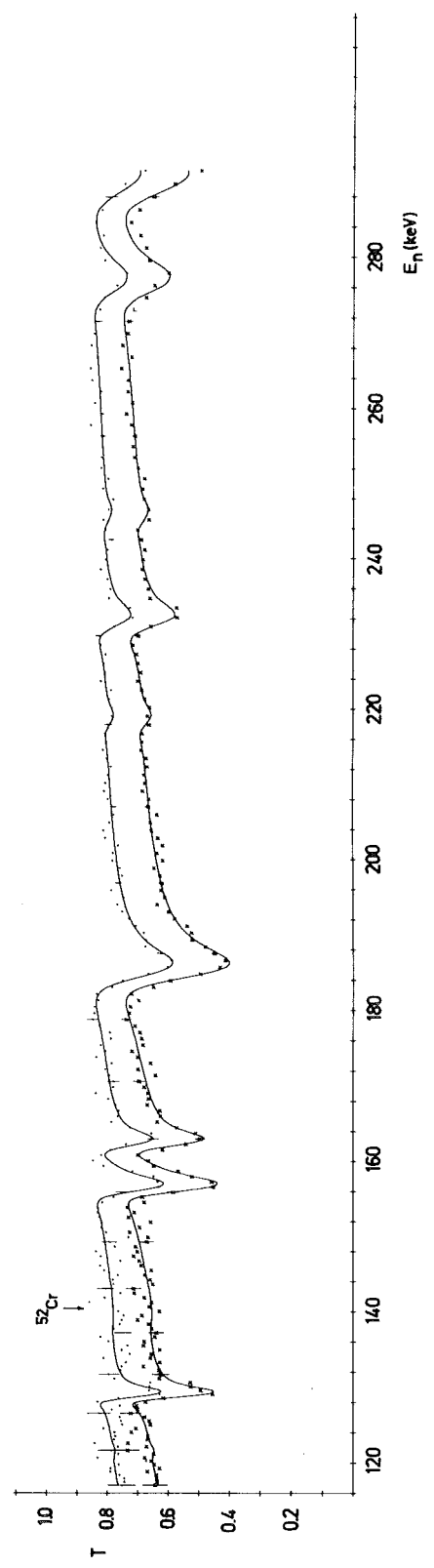
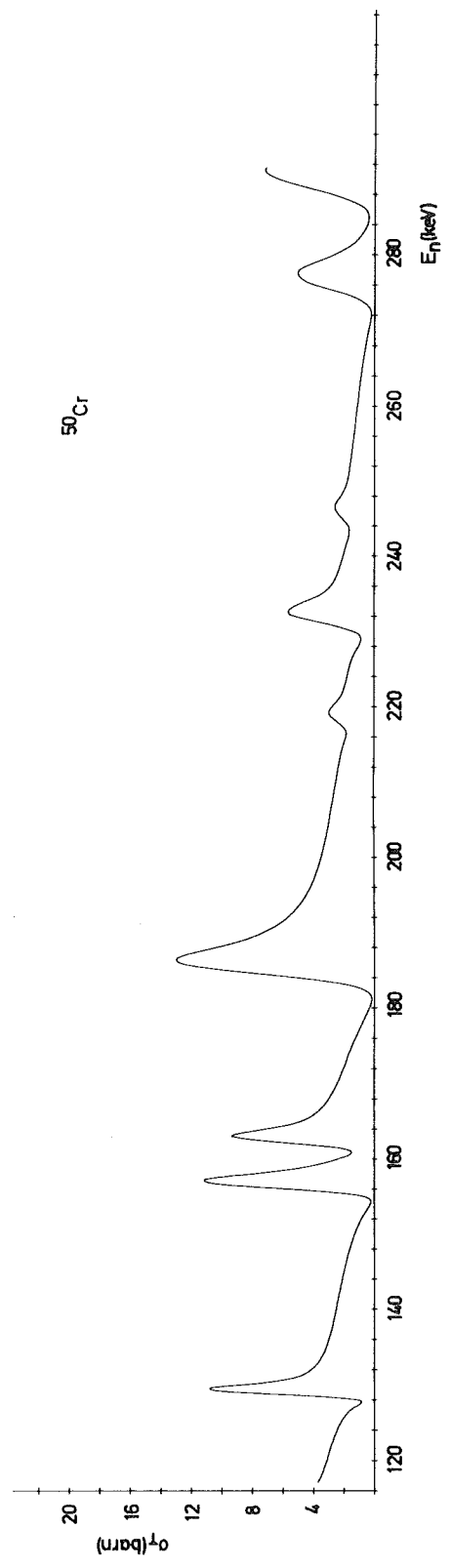
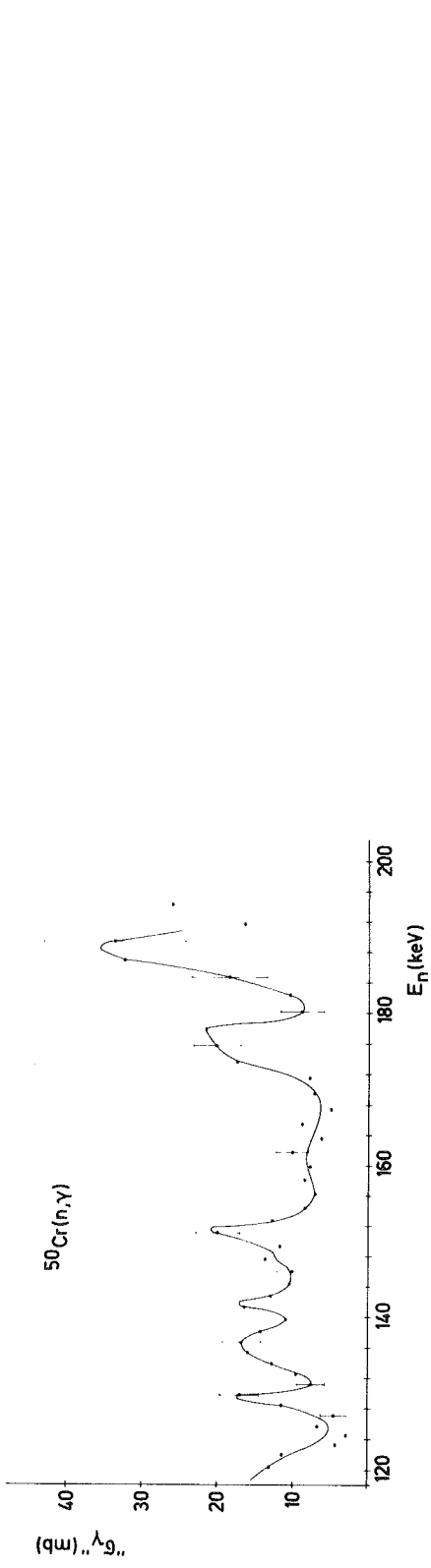


Fig. 2

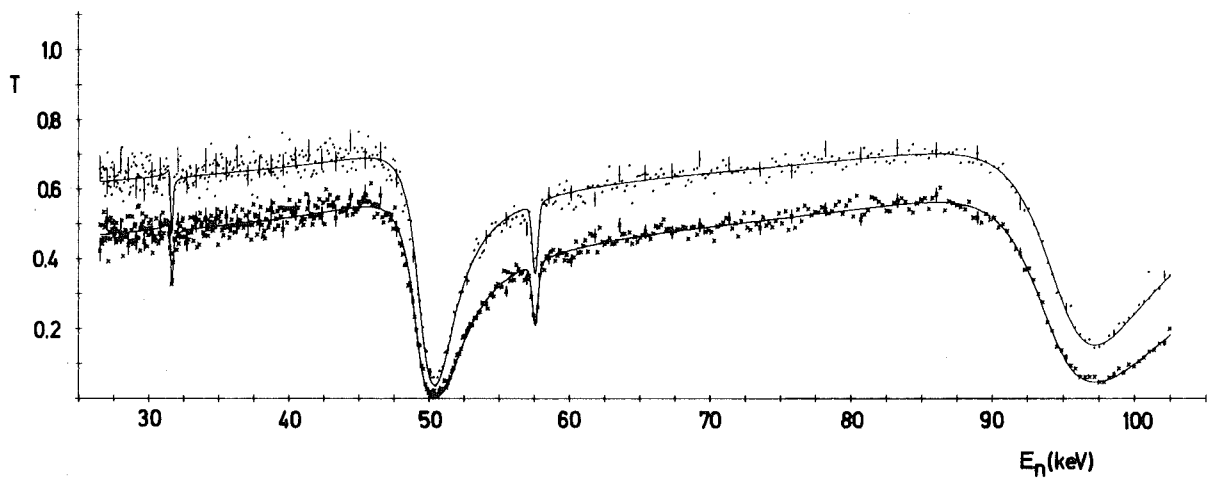
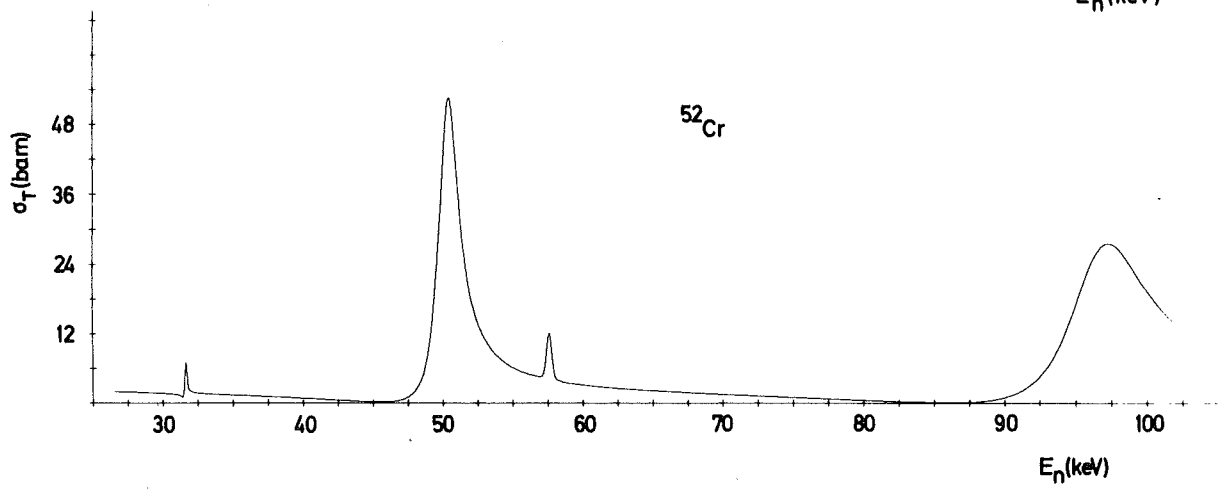
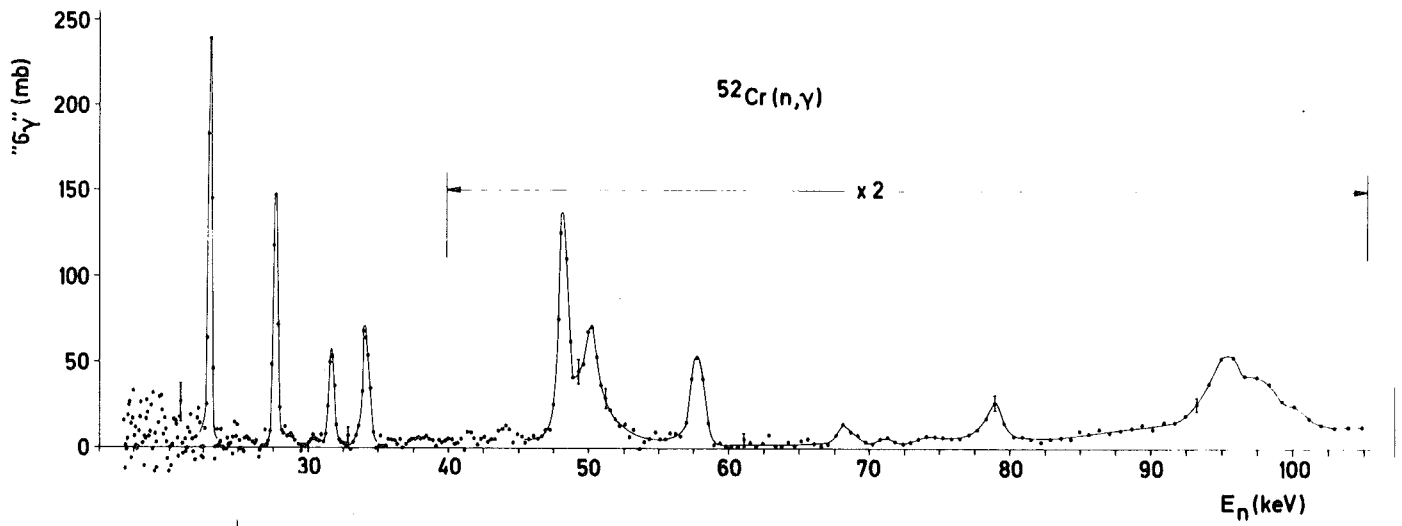


Fig. 3

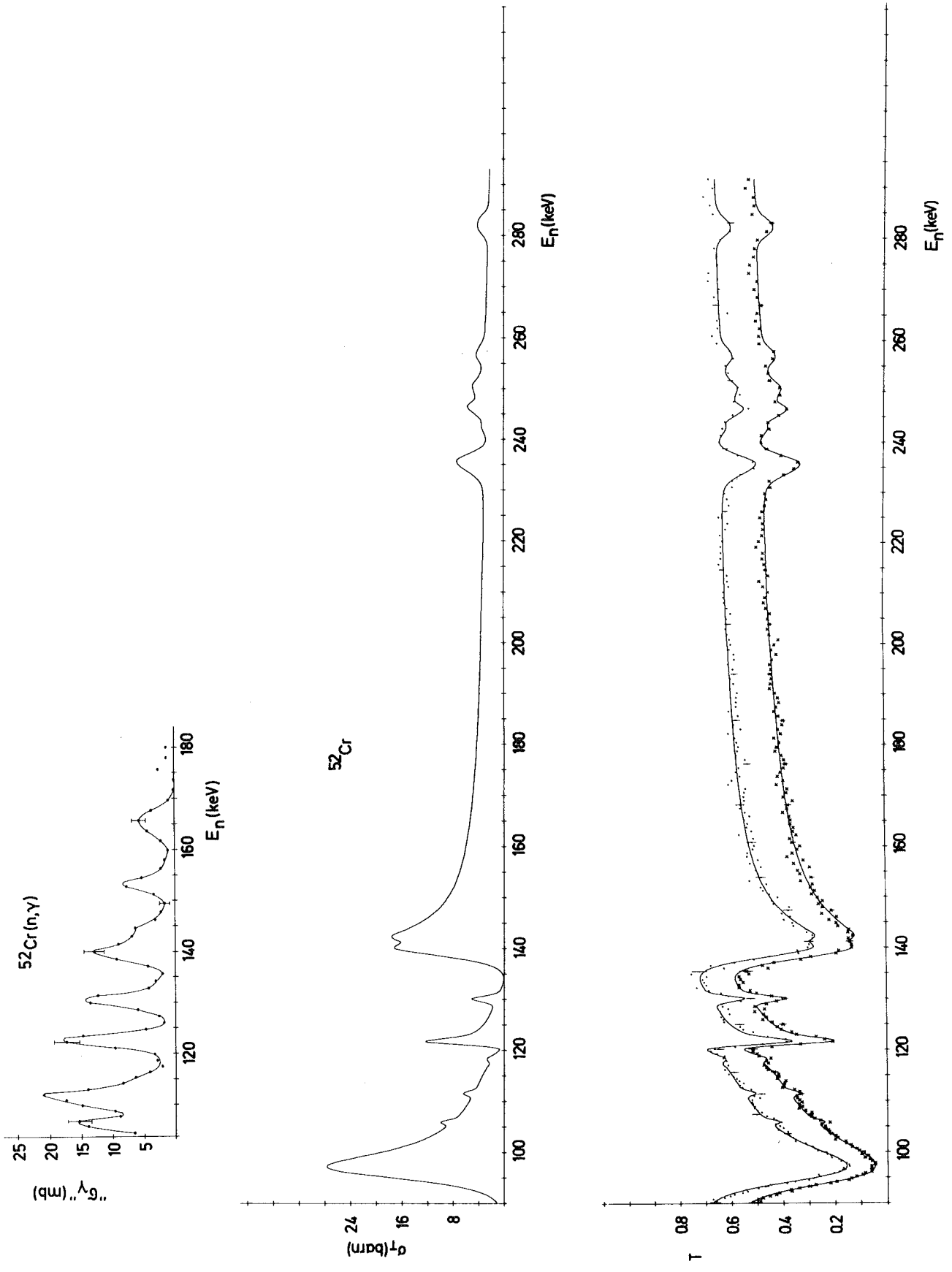


Fig.4

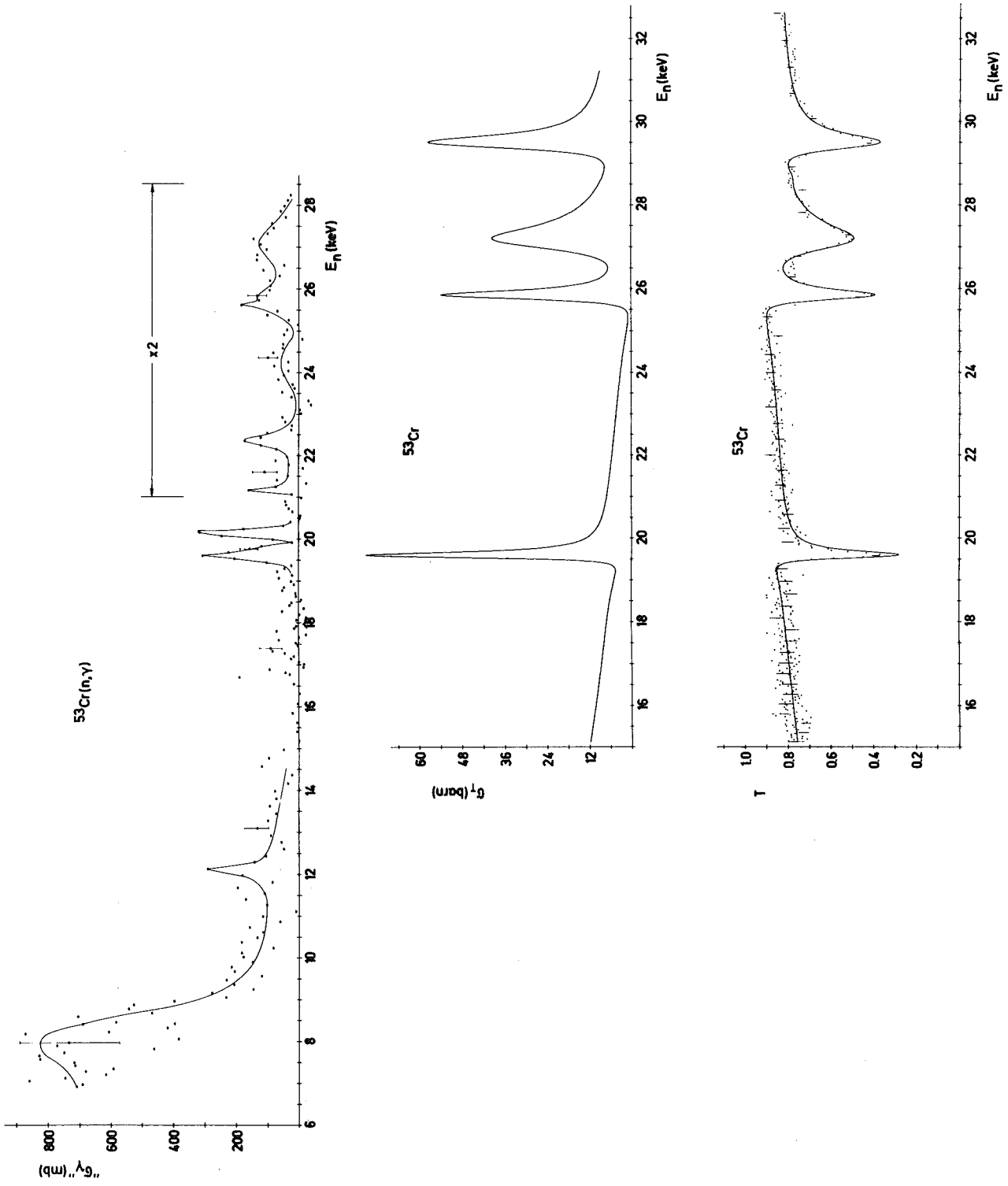


Fig.5

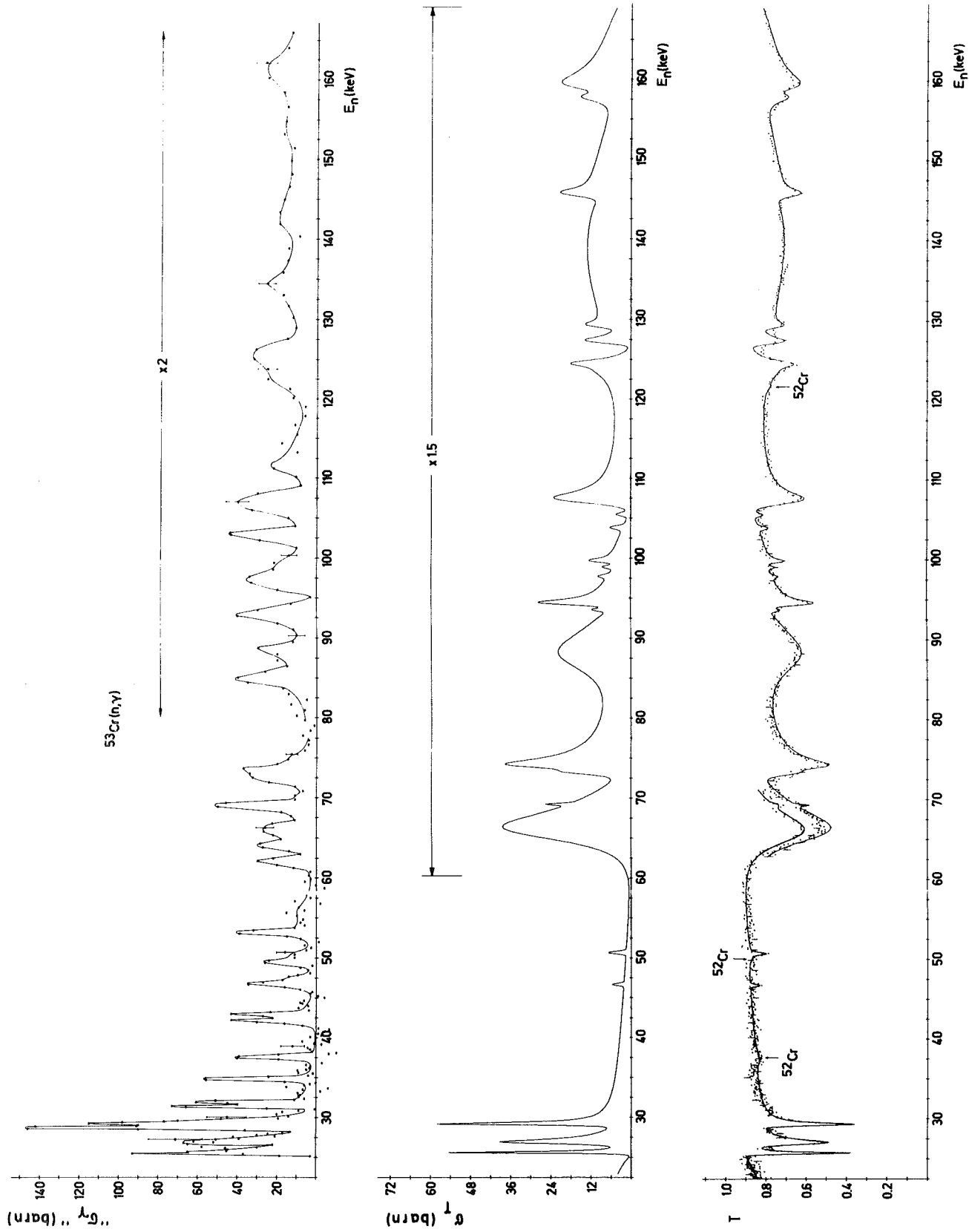


Fig.6

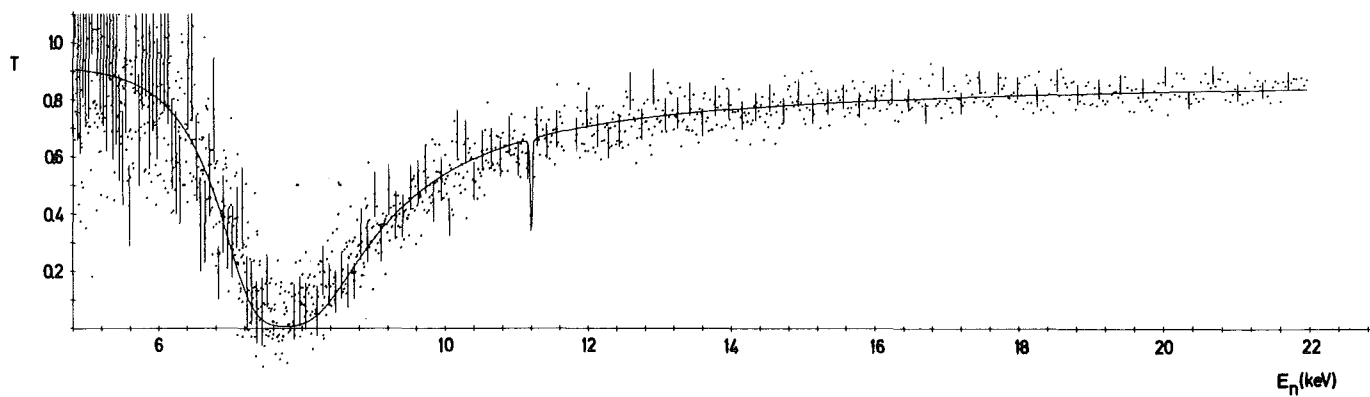
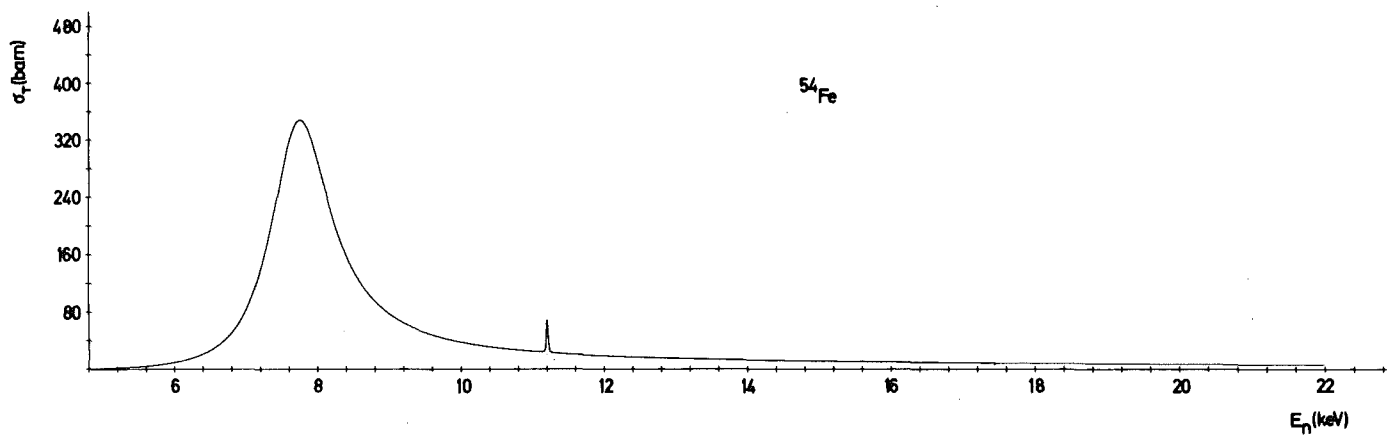
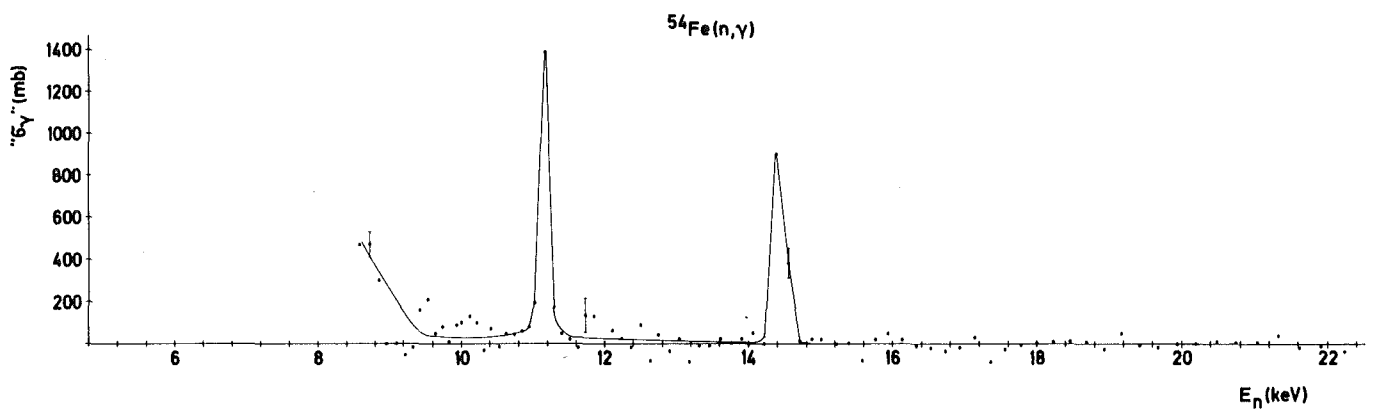


Fig.7

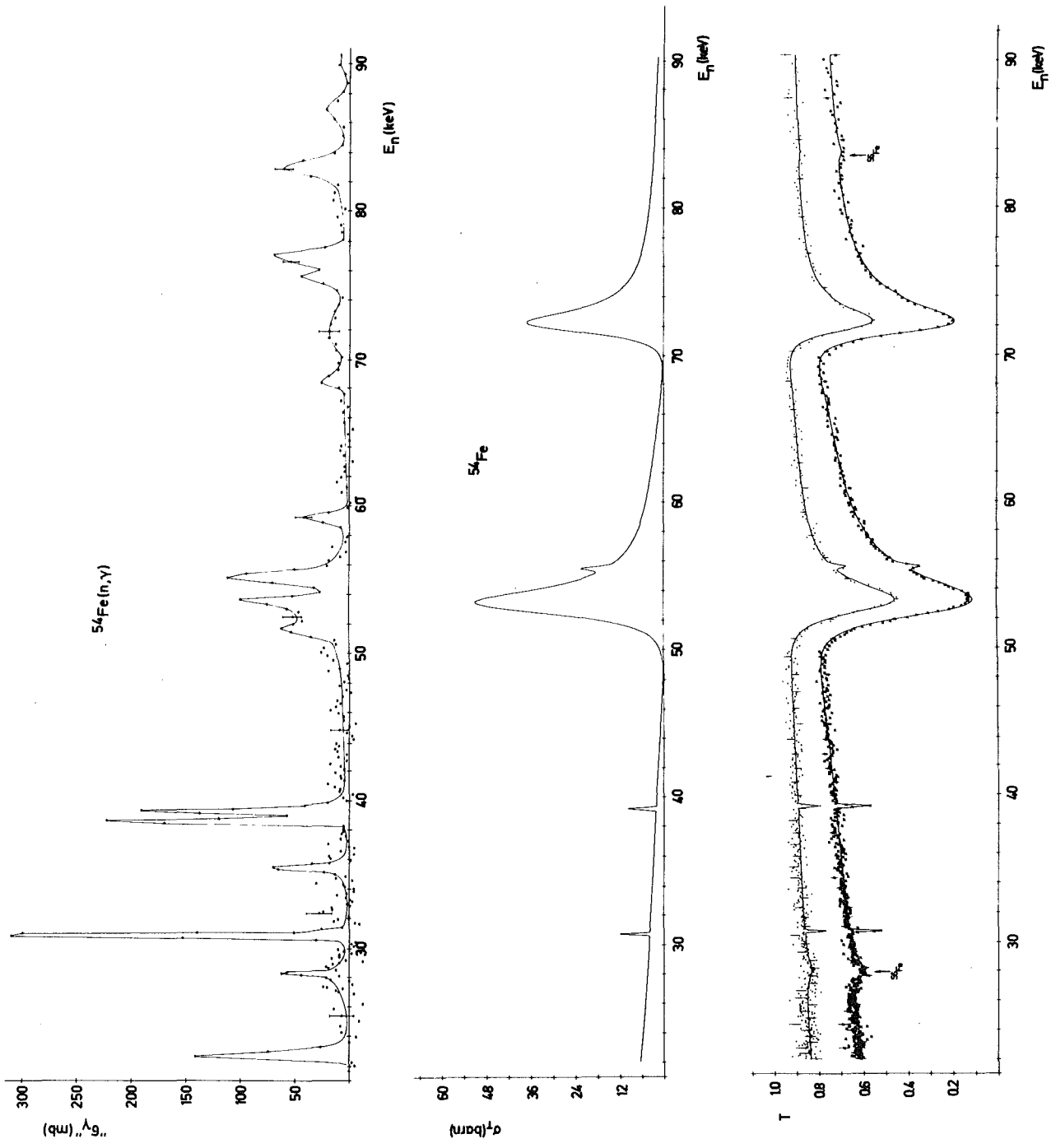


Fig.8

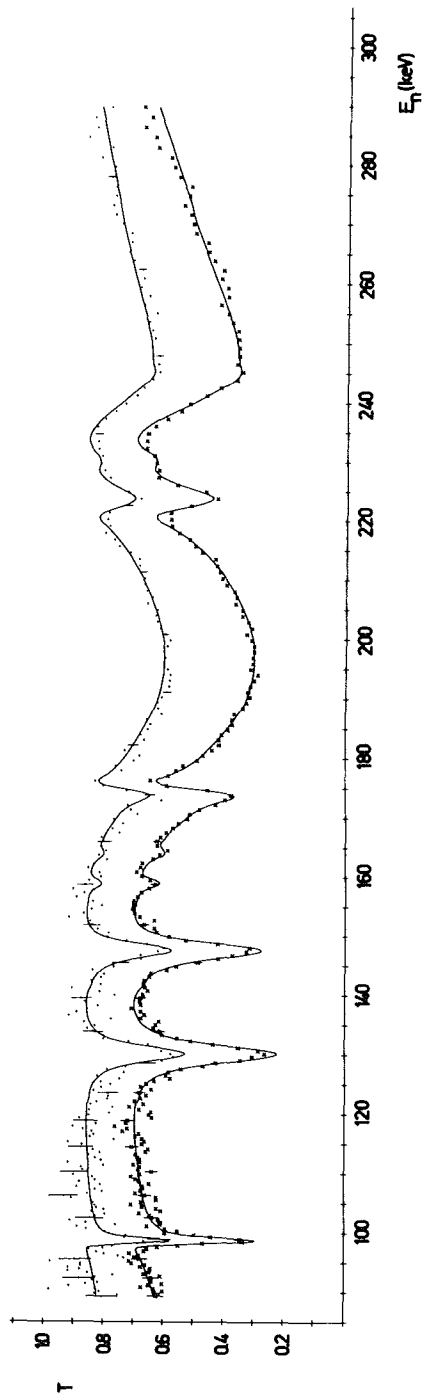
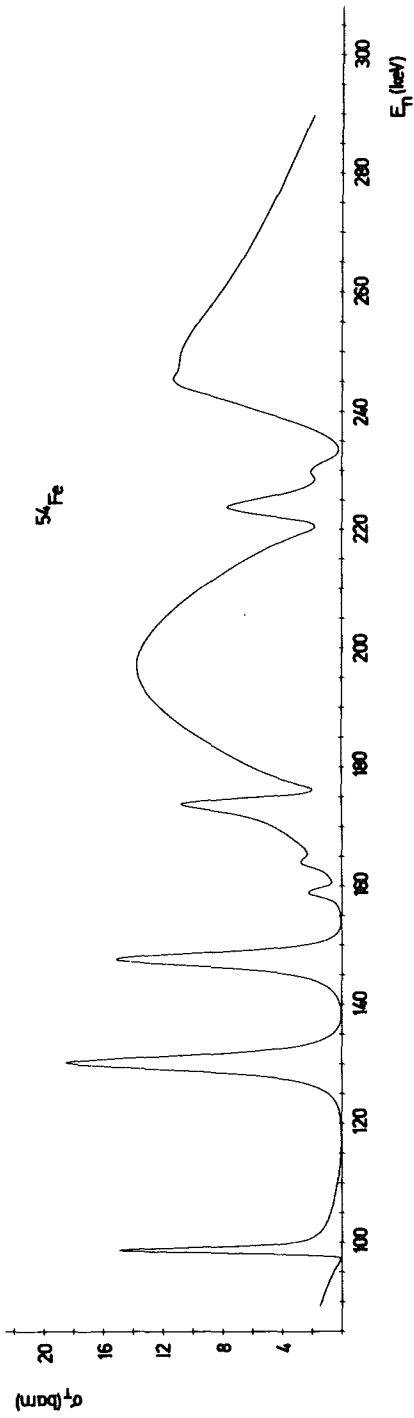
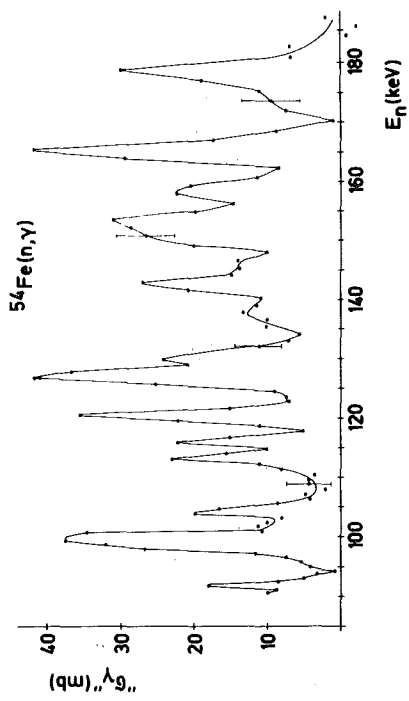


Fig.9

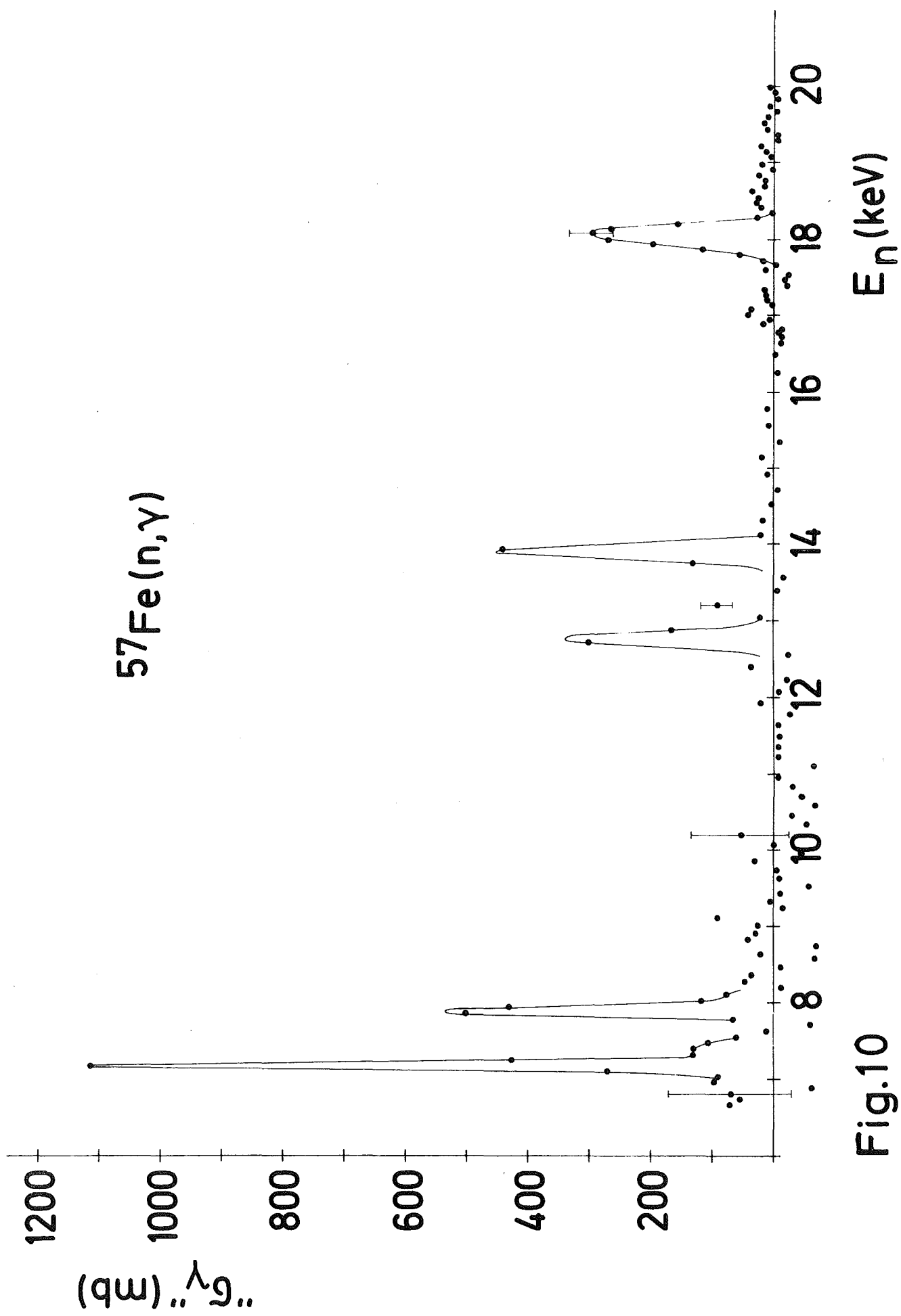


Fig.10

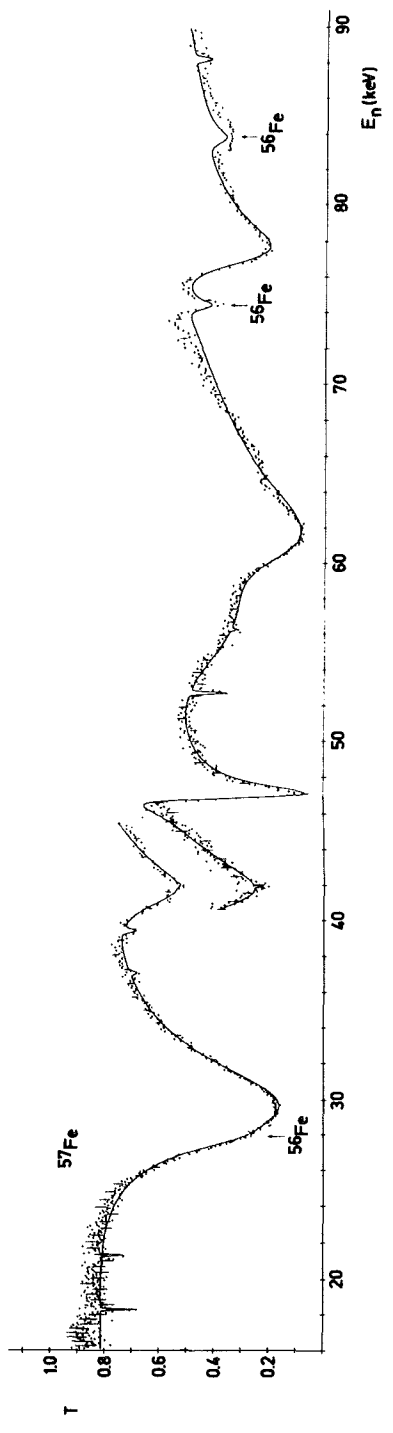
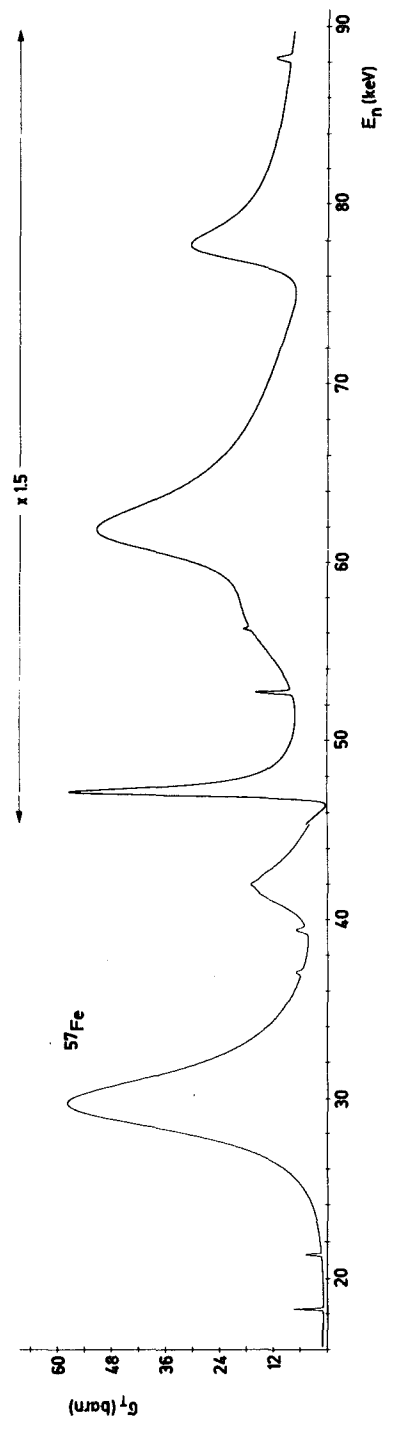
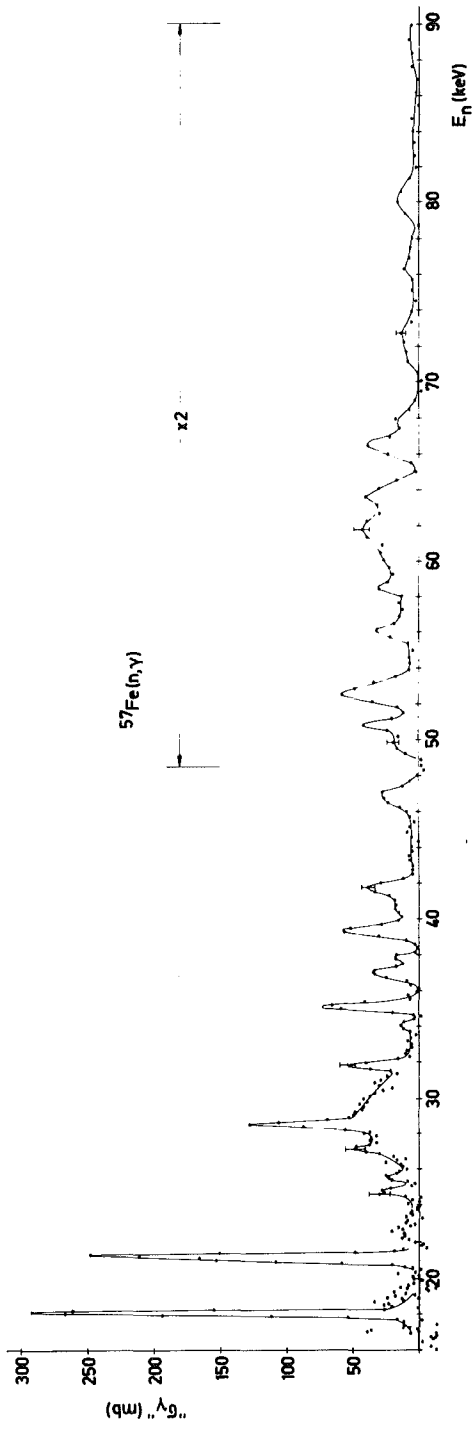


Fig. 11

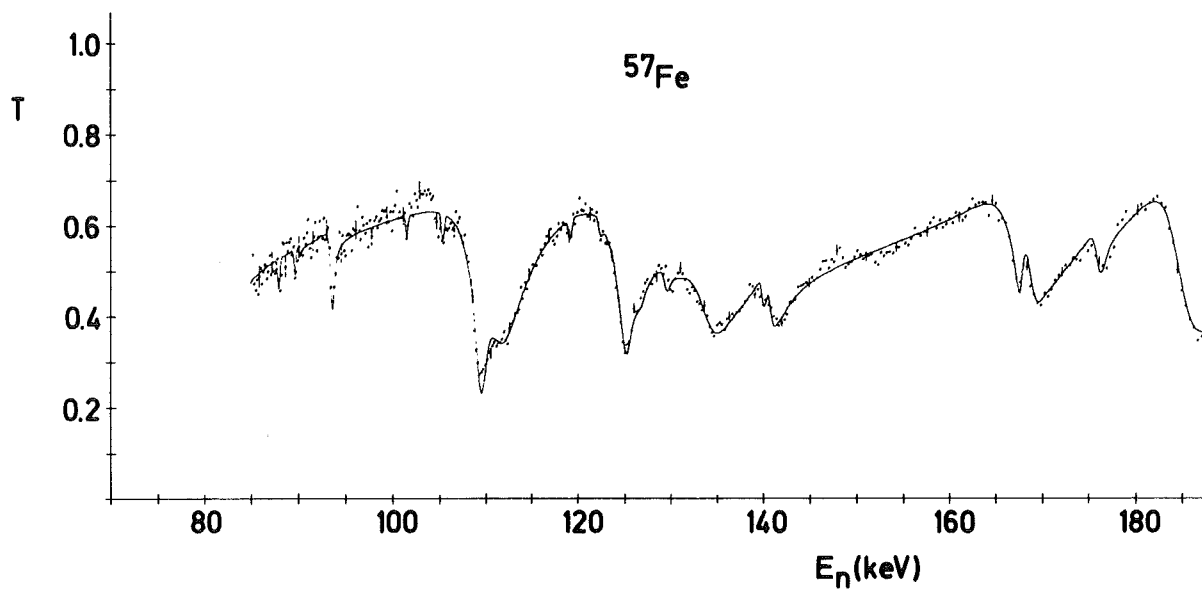
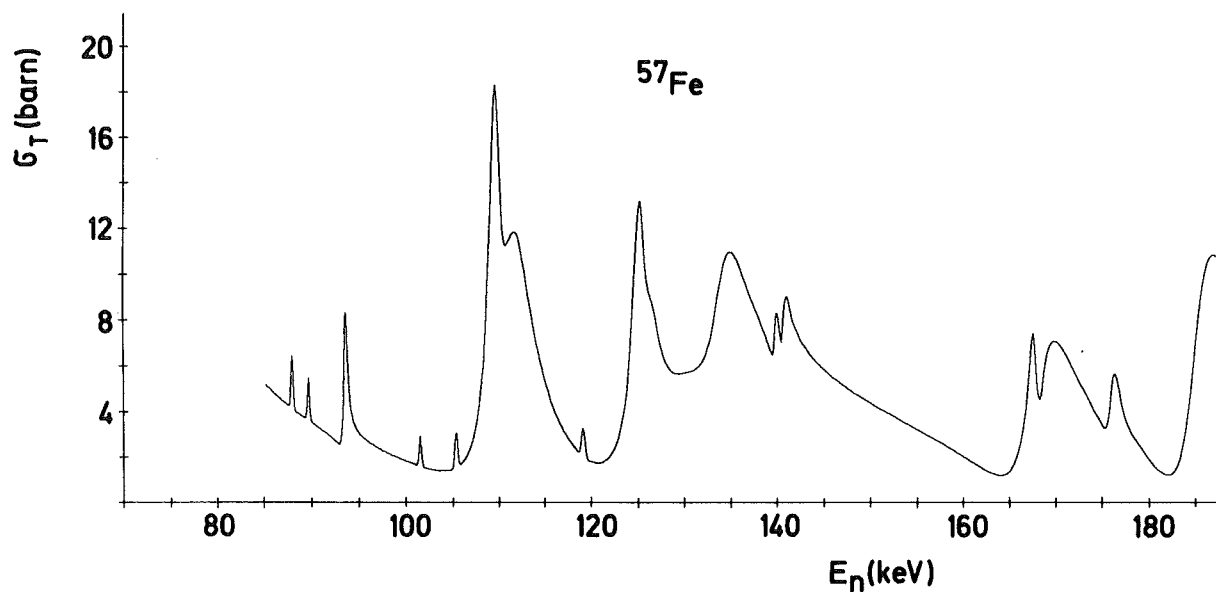
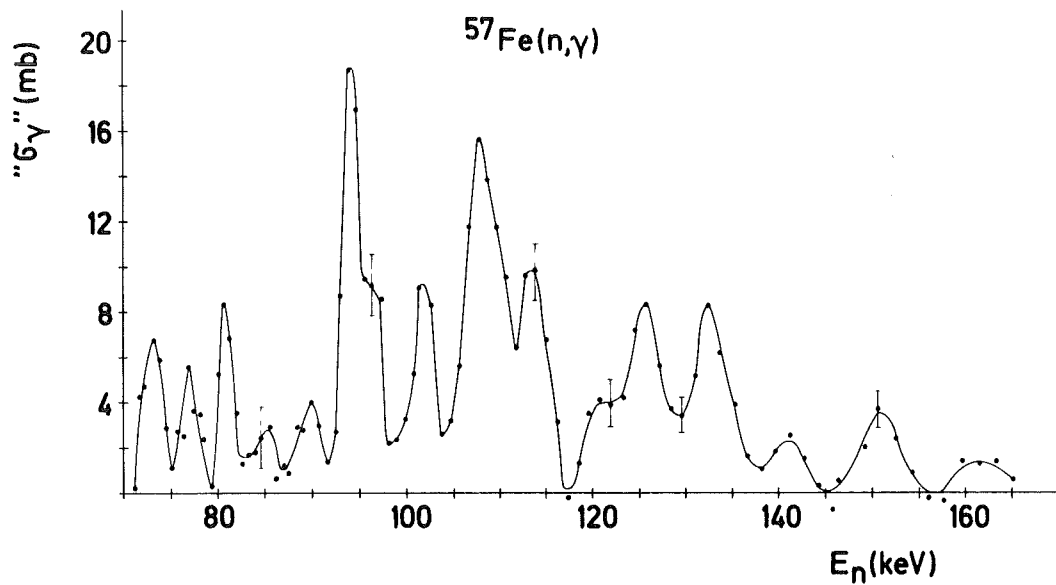


Fig. 12

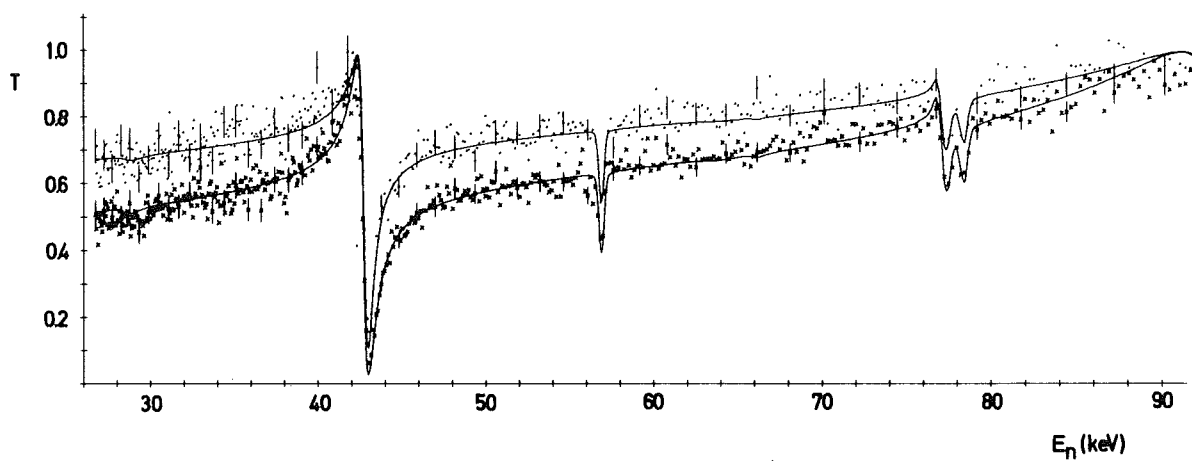
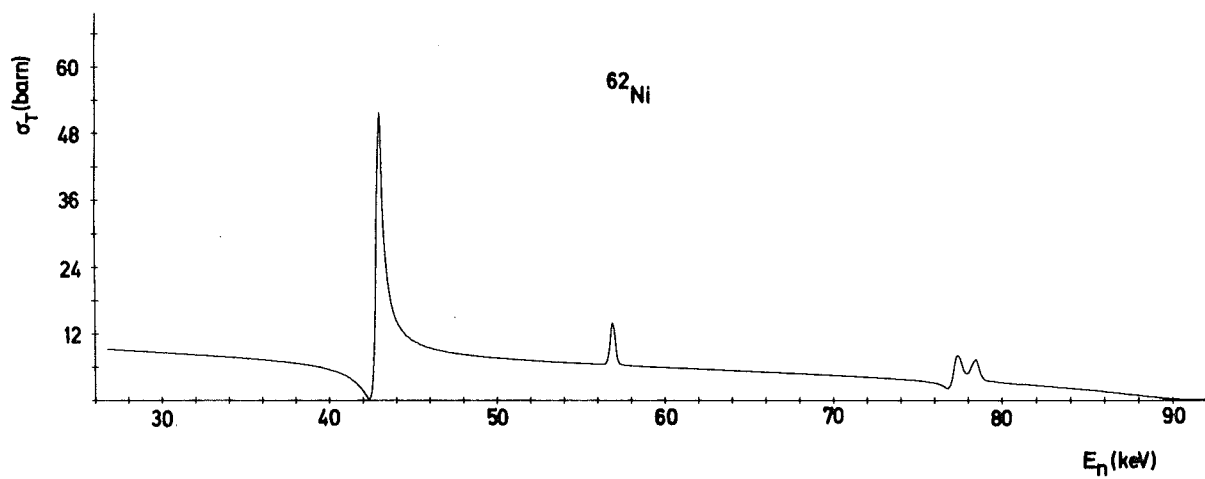
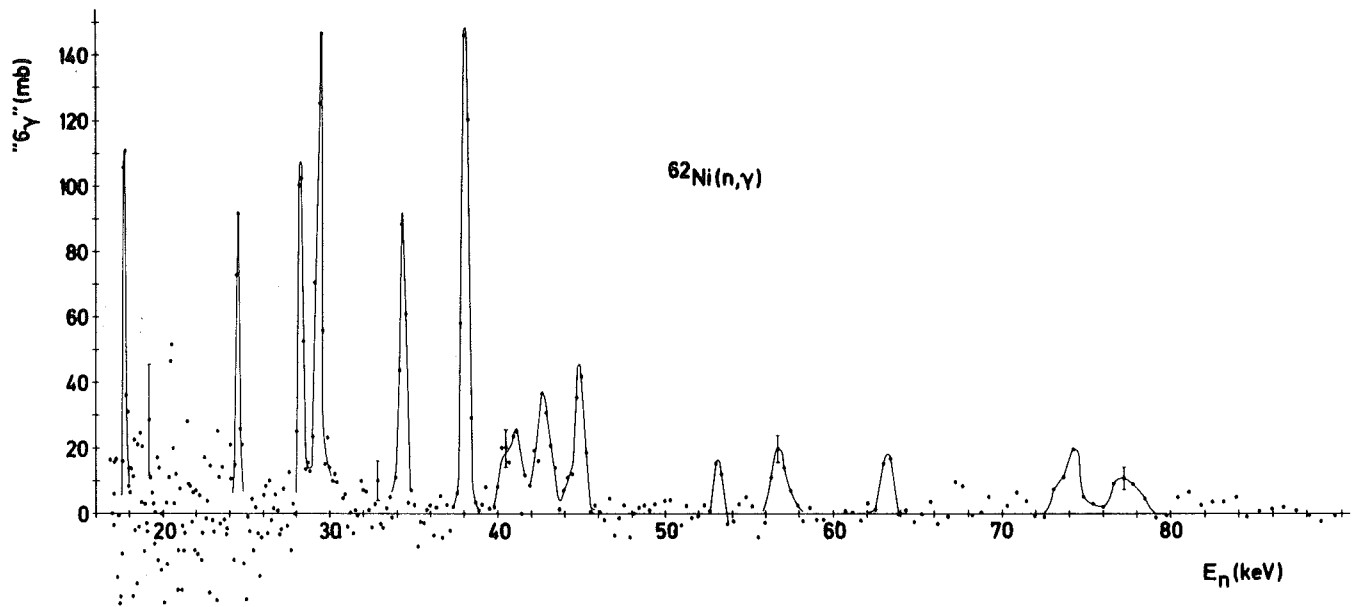


Fig.13

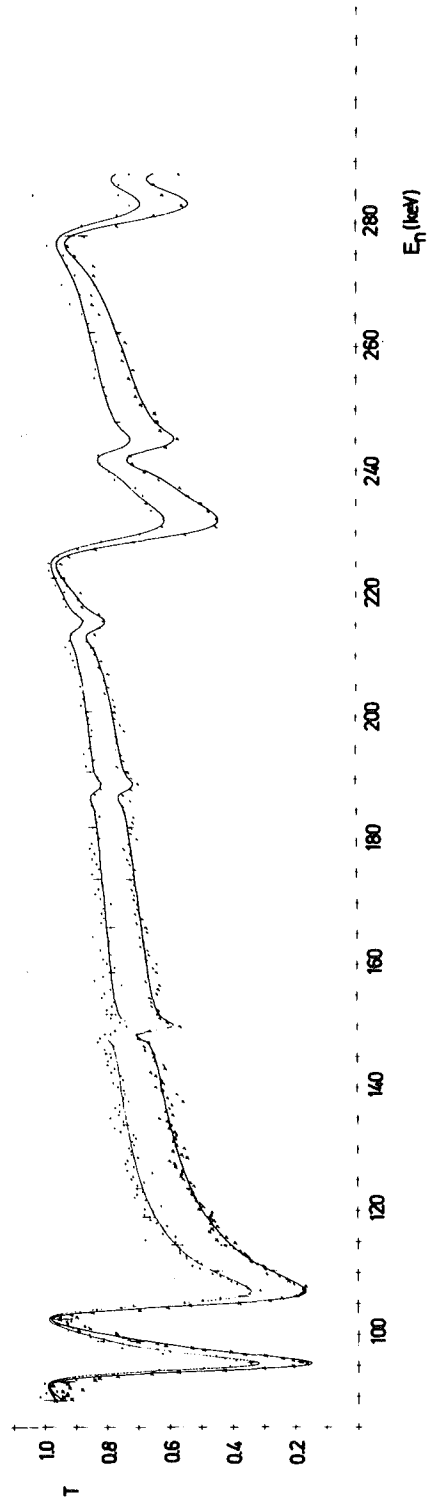
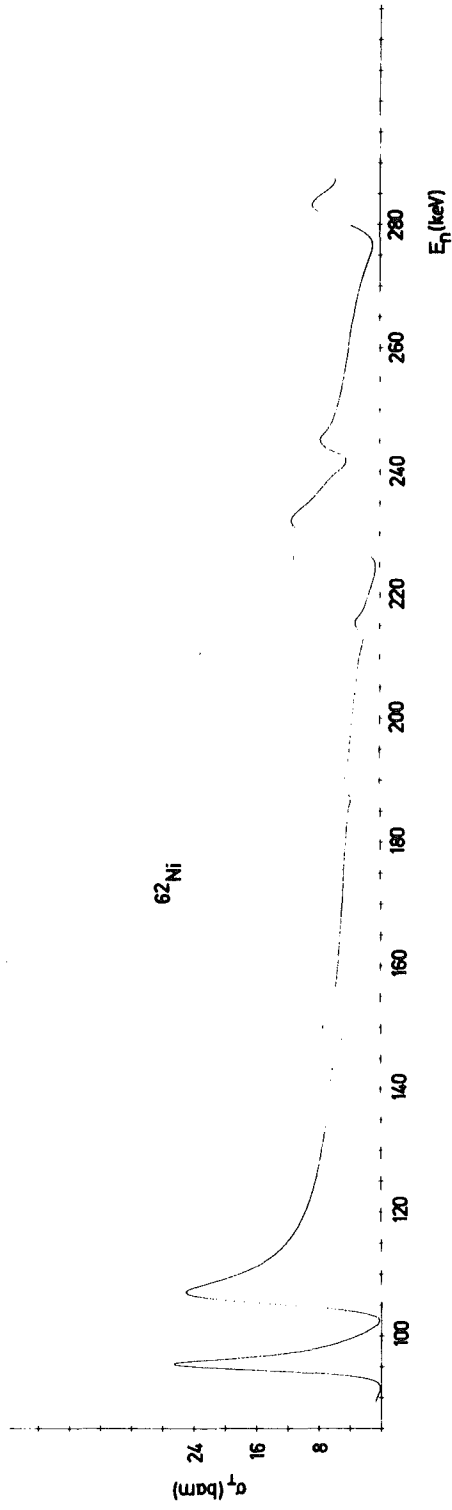
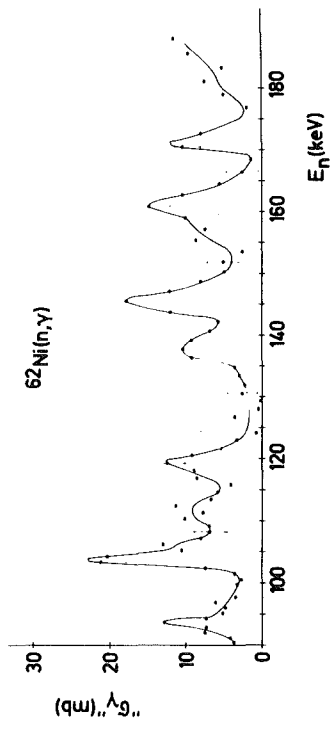
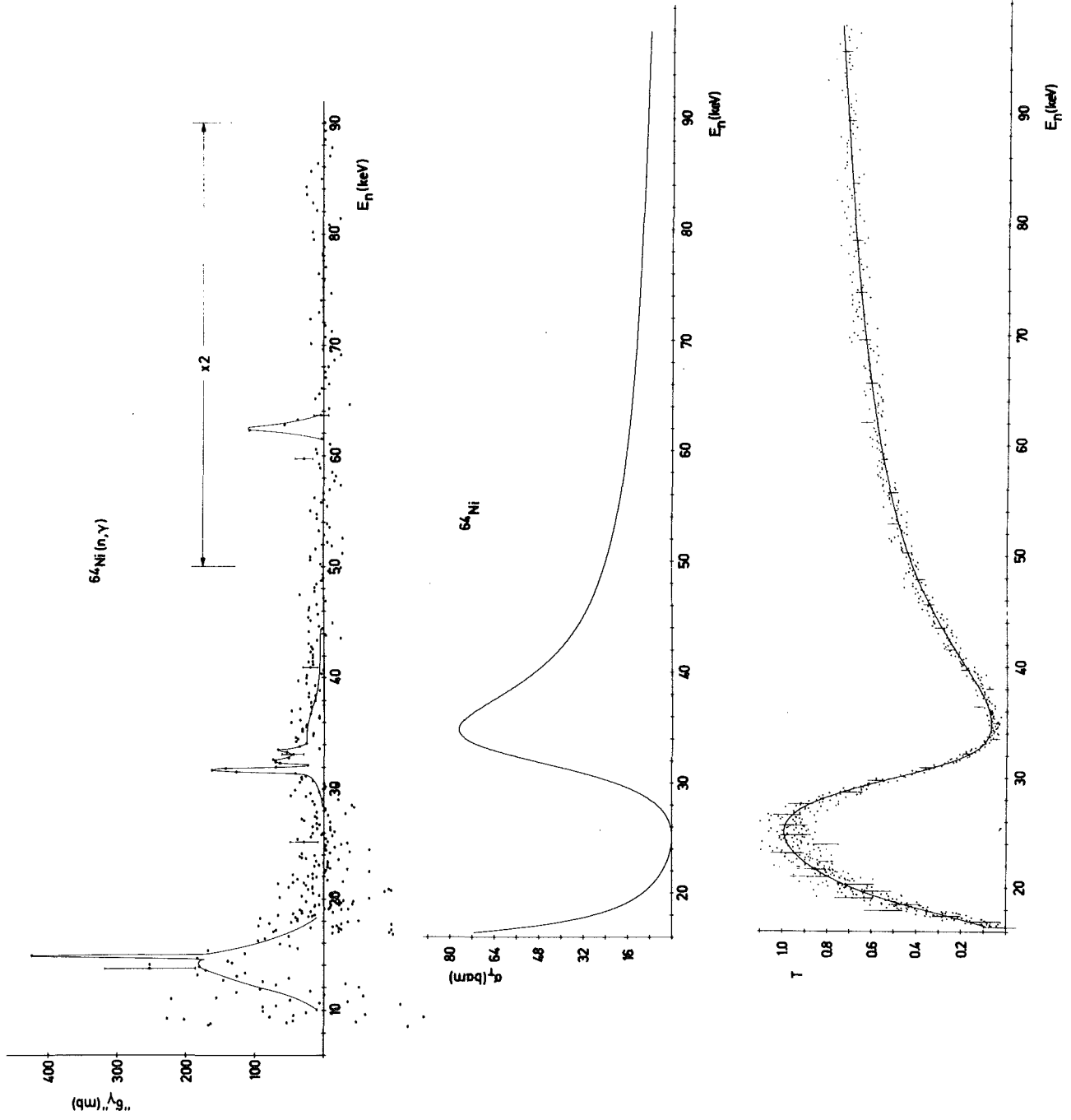


Fig. 14



**Fig-15**

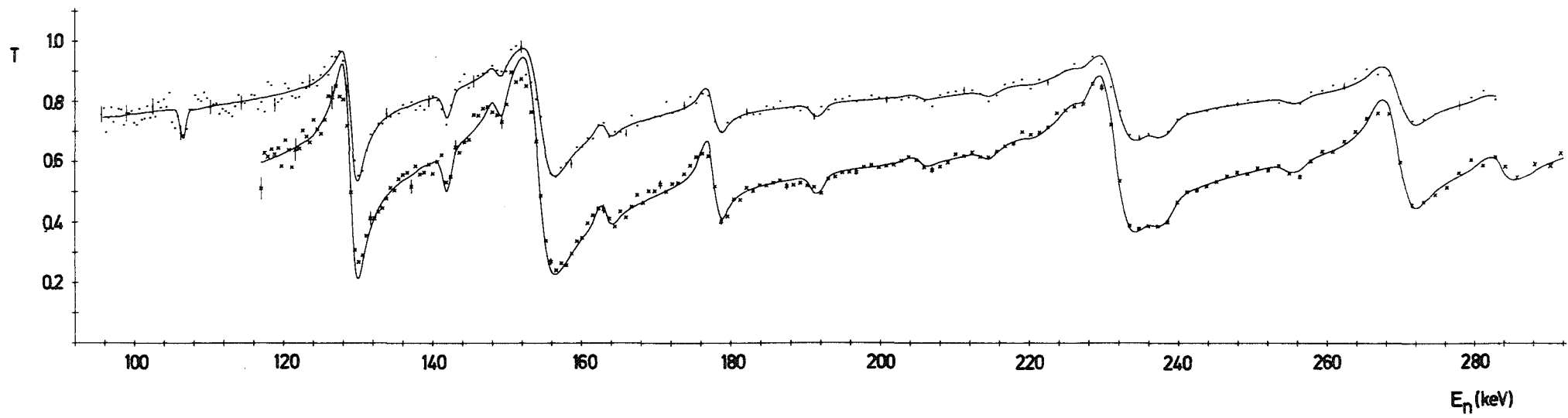
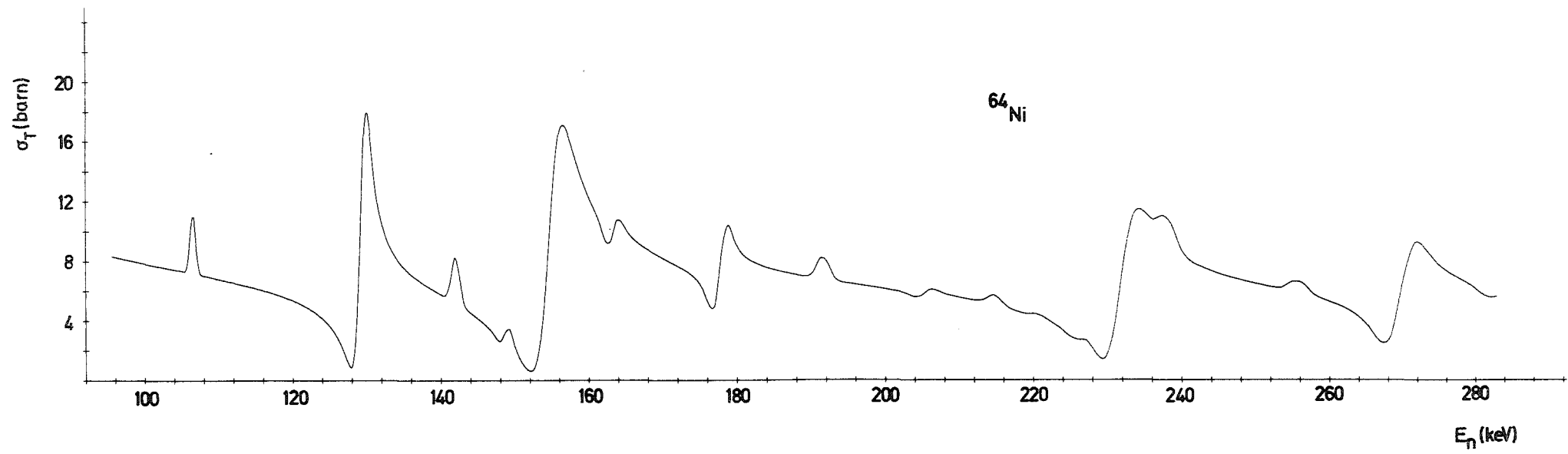


Fig. 16

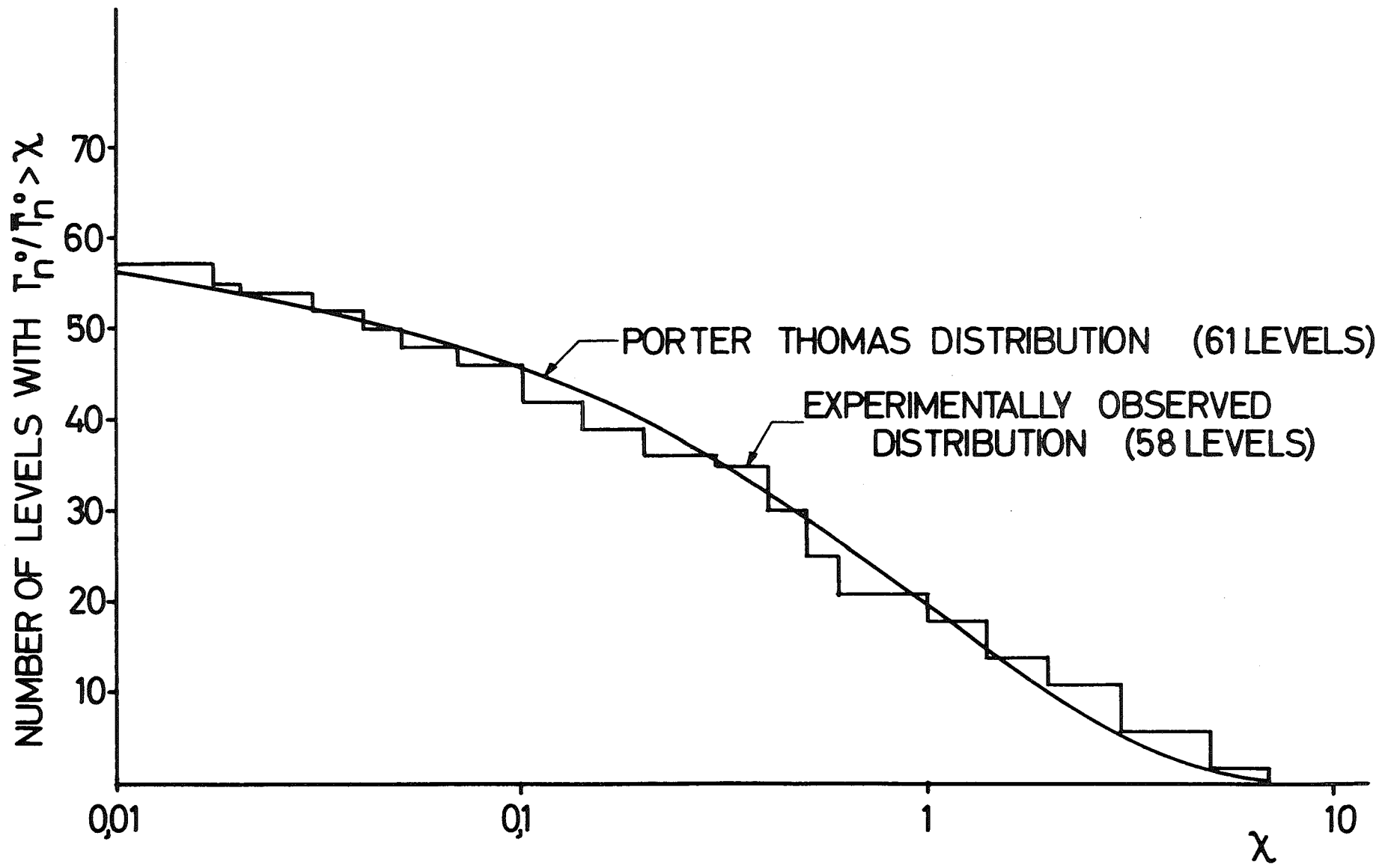


Fig. 17

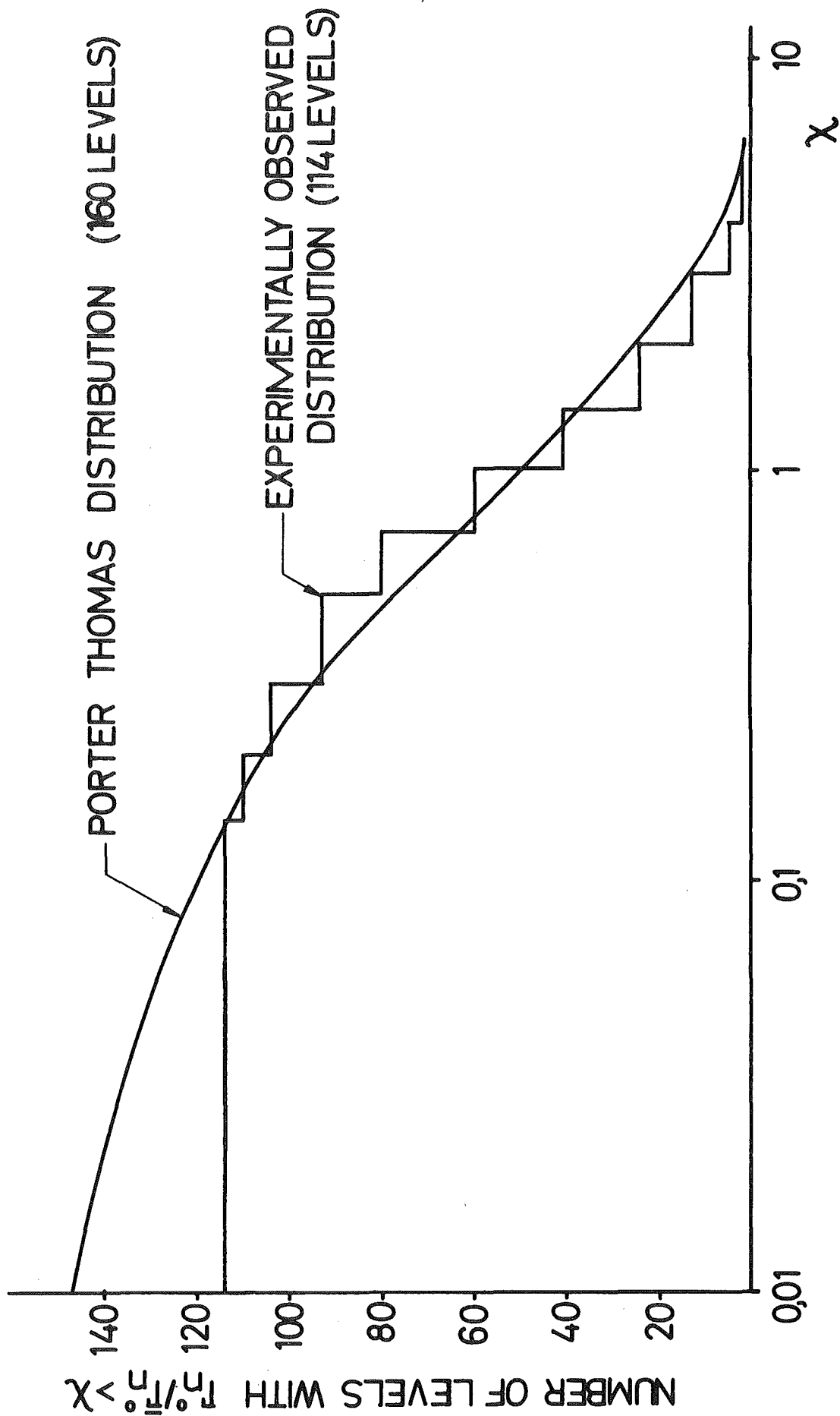


Fig.18

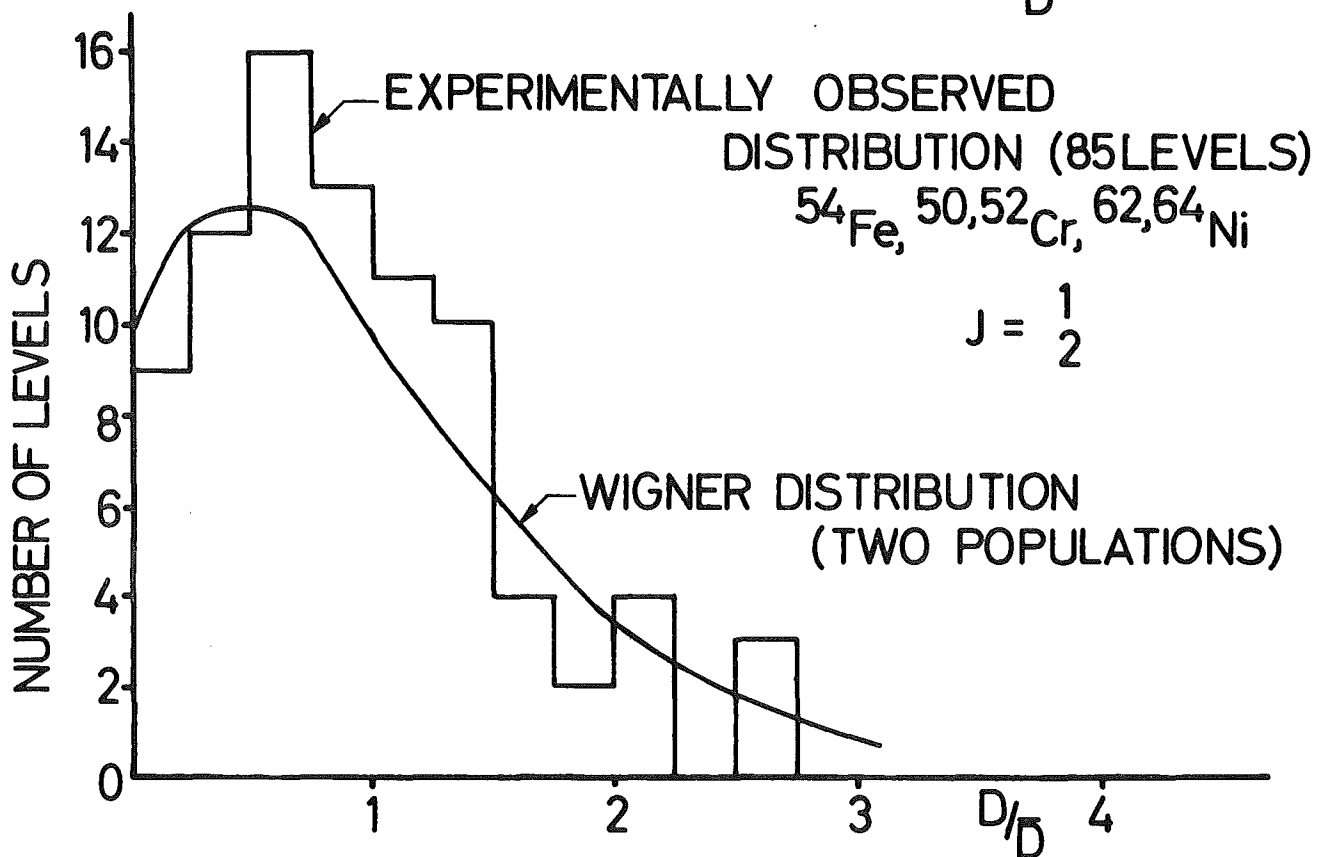
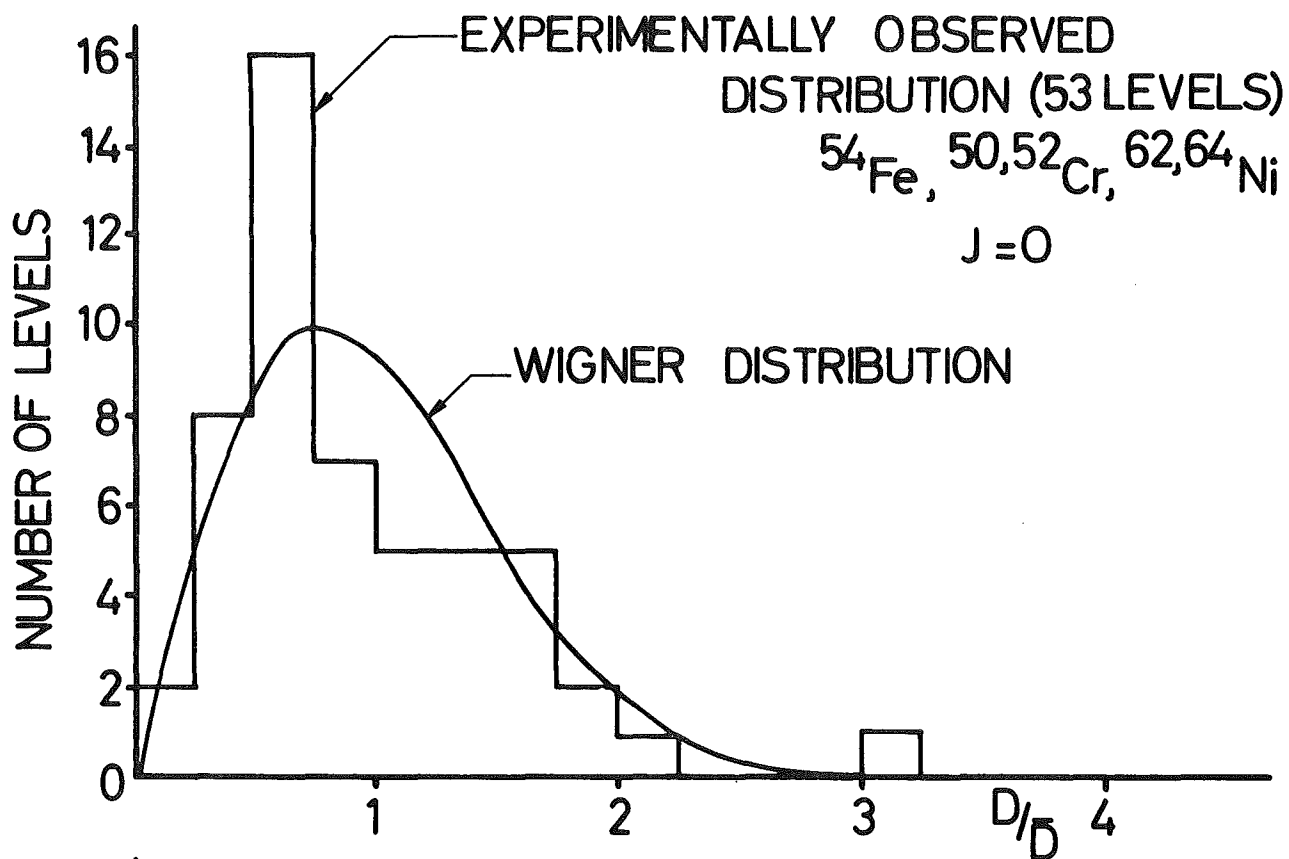


Fig.19